Response to interactive comments from Referee #1

We are a little surprised by the comments by the referee and realize that we have somehow failed to communicate what the manuscript aims to present. To this end we have revised the title, abstract, introduction and conclusions to clarify the manuscript. Besides adressing the comments, we have also made the following changes to the manuscript:

- In the previous version of the manuscript all results were reported in the units of camera pixels. We now report in physical units (meters) where appropriate.
- To obtain statistics for locations further downwind from the release point, we have included results for three more camera positions. One, camera B, at the same location as the original camera A, but with a smaller horizontal field of view, and similar cameras at about 300 m (camera B), and 500 m (camera C) downwind from the release point. For cameras B, C and D the release point of the plume is at a higher altitude to allow the cameras to see the full vertical extent of the plume. Furthermore, these cameras have more pixels in the vertical direction than camera A.
- To be able to compare the LES with the simulated images for these new camera viewing directions (viewing the plume at an elevation angle of 30.7° compared to 5.7°) new software had to be developed to calculate column densities along the camera line of sight through the LES 3D concentration.

The referee give several comments in a non-listed format. Below we have extracted the comments from the referee response and answered them one by one. The referee's comments are in italic font. The responses to the comments are shown in roman font.

Comments

- *There are no comparison with real measurements data of any kind.*

  This is modelling study with the aim to investigate whether it is feasible to derive statistics from UV camera images or not. To make this clear, we have changed the title to: 'Can statistics of turbulent tracer dispersion be inferred from camera observations of SO_2 in the ultraviolet? A modelling study'.

- *Generally speaking, the LES with the setup that the authors have chosen is not adequate to simulate plume dispersion. The grid resolution is around 1 m in all three directions and it is well known that only eddies of the size of almost ten grid cells are well resolved.*

  We investigated effects of grid resolution on plume dispersion in great detail in a recent work (Ardeshiri et al., 2020) where we used also higher resolutions. Indeed, the somewhat inadequate resolution near the source generates a larger effective source size by numerical diffusion. Unfortunately, these high-resolution simulations cannot be used because of the memory requirements of the radiative transfer model. Radiative transfer is non-local in nature and the full domain must be in memory for calculations to be efficient. Increasing the spatial resolution by a factor of 10, in 3D increase the memory demand by a factor of 1000, which is not available to us. However, the purpose of this paper is not to provide the most realistic LES results, but to demonstrate that integrated characteristic of the plume can be reconstructed accurately from camera data. And for showing this, the LES that we use is sufficient.

- *The authors use the plume from it is released until 200 meters down-stream for their investigation. Even 125 m downstream from the source the plume is not larger than ten times the grid resolution which means that the plume is not dispersing due to turbulence but rather because of the sub-grid-scale parametrisation of the LES, which I assume it more like molecular diffusion (The authors do not describe that process in detail). This means that most of the plume does not look like real*

Table 1: The mean±the standard deviation for the difference between the simulated images and the LES densities for seven (camera A) and nine (cameras B, C and D) randomly chosen time steps.

Camera	Timestep(s)	Centerline (m)	Absolute dispersion (m)	Relative dispersion (m)	Skewness
A	5, 13, 22, 31, 41, 60, 97	0.060±0.203	0.955±0.655	1.243±0.602	-0.029±0.094
B	7, 23, 32, 48, 60, 61, 65, 75 91	-0.503±1.164	-1.088±1.612	-0.240±0.565	-0.187±0.252
C	7, 23, 32, 48, 60, 61, 65, 75 91	-1.069±2.582	4.989±2.141	4.429±2.030	-0.159±0.794
D	7, 23, 32, 48, 60, 61, 65, 75 91	-0.353±2.851	7.658±1.839	7.036±1.681	0.505±1.375

dispersion but appears much smoother. It is therefore dubious to replace experimental measurements with LES in this case.

We are well aware of the effects of numerical and sub-grid-scale diffusivity, see also answer to previous question. Furthermore we have revised our results to use world coordinates instead of pixel coordinates. Revised results for the camera in the original manuscript are shown in Fig. 1. We note that at the horizontal angle of 90°, corresponding to about 110 m downstream from the release point, the plume is already about 4-5$\times\sigma_r \approx 16-20$ m. Thus, already at 110 m downstream the actual plume size is much larger than the LES voxel size.

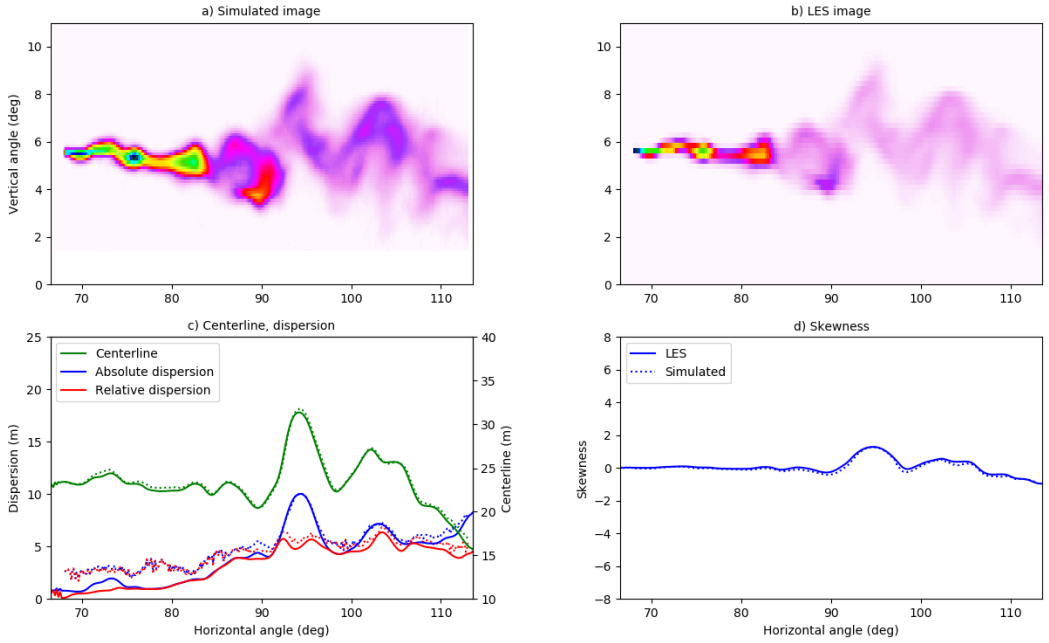

Figure 1: a) The plume apparent absorbance. b) The LES column density integrated along the line of sight. Colorscales in a) and b) are relative and thus no colorbars are provided. c) The centerline, absolute and relative dispersions. d) The skewness. The solid lines are LES results and dotted lines are values calculated from the simulated images.

We have made simulations for cameras seeing the plume further downstream, Fig. 2.

One example for camera D is shown in Fig. 3. We have updated the table describing the reference comparison to include the results for the new cameras, see Table 1. The manuscript have been updated with these new results and corresponding discussions.

Finally, the sub-grid-scale treatment of the LES is described by the following senence in section 2.1 of the manuscript:

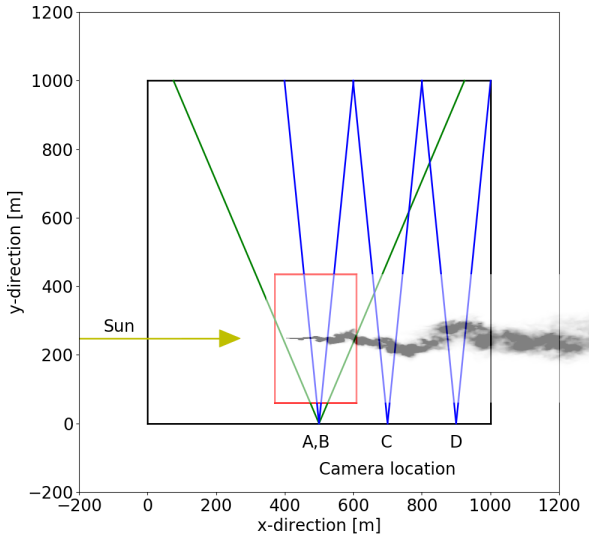

Figure 2: Bird's eyes view of the 3D domain (black square) and the SO_2 plume location within the domain (red square, for camera A simulation, shifted along x-axis for the other cameras). The UV cameras are located where the two green or blue lines intersect. The lines indicate the horizontal field-of-view of the cameras. The column density of the plume is included for illustrative purpose. The direction of the incoming Sun ray is shown by the yellow line.

> In this methodology, the large scales of the turbulent flow are explicitly simulated while a low-pass filter is applied to the governing equations to remove the small scales information from the numerical solution. The effects of the small scales are then parameterized by means of a sub-grid scale (SGS) model (e.g. Deardorff, 1973; Moeng, 1984; Pope, 2000; Celik et al., 2009).

- *Then the authors go to radiative transfer calculations with the sun as the light source. It is rather surprising that the calculations use circular boundary conditions such that when one photon leaves the domain on one side it appears again on the opposite side. The refer to energy conservation for this, but I simply dont understand the reasoning behind. It appears unphysical and gives rise to various artefacts such as ghost plumes that have to be removed.*

  The radiative transfer model used is based on the Monte Carlo technique and trace photons through the model-domain (the atmosphere). The model-domain is a rectangular cuboid. With a solar source the photons enter the domain through the top surface. Photons are traced until they leave the domain or are absorbed. If a photon leaves the domain through one of the four sides it is lost and will remain unaccounted for, and hence energy conservation is broken which might lead to non-physical results. Thus, to quote Mayer (2009):

  > If a photon leaves the model domain through the side, we apply periodic boundary conditions: the photon re-enters at the opposite side; this ensures energy conservation and is appropriate for most applications, given that the model domain is large enough so that the process under consideration are not affected by edge effects.

- *They analyse only one (!) out of the 100 snapshots which I think is a very little number for getting good statistics.*

  This statement is not correct. In Table 1 of the manuscript statistics based on 7 snapshots are presented. In addition we have now also performed simulations for more cameras, see Table 1. For the sensitivity analysis, however, only one snapshot is used. Though, there is no physical reason

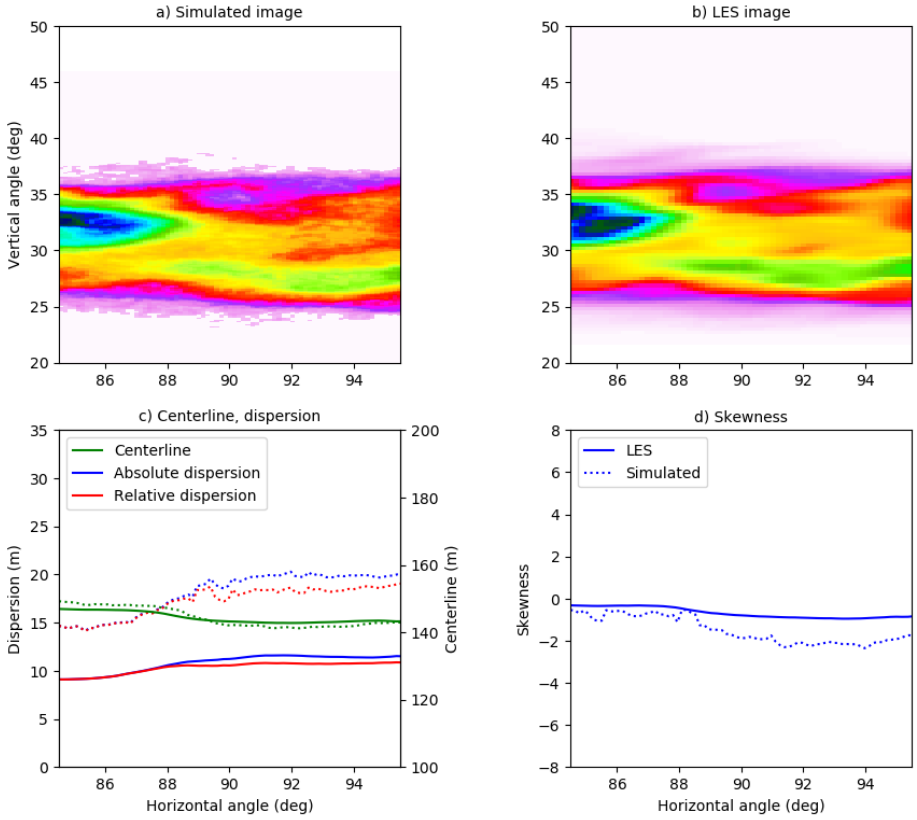

Figure 3: Results for Camera D and time step 91. a) The plume apparent absorbance. b) The LES column density integrated along the line of sight. Colorscales in a) and b) are relative and thus no colorbars are provided. c) The centerline, absolute and relative dispersions. d) The skewness.

for the results from the sensitivity analysis to be different if other or more snapshots are used. Also, note that if the instantaneous spatial statistics are correct, the ensemble statistics will also be correct. This is not necessarily true the other way around. We have revised the abstract and the introduction part of the manuscript to make this clearer.

- *The plume statistics analysis is a bit messy. There is an equivalence between the x and z position in space and the two pixel coordinates in the camera. This might be a good approximation but it is confusing that the same symbols are used for the different physical quantities. The mean plume height is a mean of plume heights at all downstream positions. Usually, in a boundary layer the mean plume height is a function of downstream position x since the plume may rise if it is released close to the surface. As a consequence of choosing the average plume height over all x values is that the absolute dispersion sigma$_z$ is a mix of ordinary absolut dispersion (which is relative to the mean height at a specific downstream position x) and the general plume rise. The definition of meandering dispersion suffers some of the same inconveniences. The poor reason for those somewhat awkward definitions is that the authors have an ensemble of one which prevents making ensemble means as is usually done.*

  In the revised manuscript we do not use pixel coordinates, but world coordinates x and z throughout. Furthermore, as pointed out by the referee: The absolute dispersion can be properly defined only using an ensemble or time average. This is not possible here as we do not have an esemble available. We thus adopt the center of the source ($\overline{z} = z_0$) as the reference vertical position and define the absolute dispersion accordingly. It is noted, that with this definition of the absolute position, relative and absolute dispersion are correctly the same at the source location, since meandering

here is zero. The revised statistics are shown in Fig. 1.

- *Jumping to fractal dimensions, the authors fail to describe exactly what they do, and one could ask how relevant fractal dimensions are given the poor resolution of the LES. Often fractal dimensions are used to describe the interface between the plume and the surrounding air, but here it is unclear what N(epsilon) really is. There is no supporting figure to let the reader know.*

  In response to the comment we have decided to leave this section out.

- *The lack of realism of the LES of the plume is also displayed in figure 4 where the relative dispersion is shown. The slope of the red curves in this double logarithmic plot around 1/2 indicating pure molecular-like dispersion (if it is sigma$_{zr}$ which is plotted). It is confusing that the authors talk about slope between 0.01 and 0.0217 while I get something from the plot around 1/2. Theoretically, the slope in this range should be close to 3/2 as also mentioned in the Dinger et al paper which they refer to.*

  In response to the comment we have decided to leave this section out.

- *To summarize, it looks like the work does not spend enough computational resources on doing a realistic dispersion simulation and, secondly, doing analysis of all their snap-shots to get proper statistics.*

  As discussed briefly above, and fully discussed in Ardeshiri et al. (2020), the LES simulations are not perfect, despite this the grid resolution preserve qualitative characteristic similar to more resolved simulations. Indeed in Ardeshiri et al. (2020) it is demonstrated that concentration PDF of the coarser resolution simulations has the same shape but with less fluctuations. As mentioned in the manuscript, and further explained above, it is not computationally feasible to perform radiative transfer simulations for all snap-shots. Nor is it required to reach the aims of this manuscript. Both these points have been emphasized in the revised manuscript.

- *Turbulence is one of the unresolved problems of physics it is written at several occasions. It is not very clear that this work brings us much further.*

  This sentence has been removed throughout the manuscript.

Bibliography

Ardeshiri, H., Cassiani, M., Park, S., Stohl, A., I.Pisso, and Dinger, A.: On the convergence and capability of large eddy simulation for passive plumes concentration fluctuations in an infinite-Re neutral boundary layer, Boundary-Layer Meteorol., accepted for publication, 2020.

Celik, I., Klein, M., and Janicka, J.: Assessment measures for engineering les application, J. Fluid Eng, 131(3), 031 102, 2009.

Deardorff, J.: The use of subgrid transport equations in a three-dimensional model of atmospheric turbulence, J. Fluid Eng, 95, 429–438, 1973.

Mayer, B.: Radiative transfer in the cloudy atmosphere, Eur. Phys. J. Conferences, 1, 75–99, 2009.

Moeng, C.: A large-eddy simulation model for the study of planetary boundary-layer turbulence, J. Atmos. Sci, 41, 2052–2062, 1984.

Pope, S. B.: Turbulent Flows, Cambridge University Press, 2000.

Response to interactive comments from Referee #2

Besides adressing the comments, we have also made the following changes to the manuscript:

- In the previous version of the manuscript all results were reported in the units of camera pixels. We now report in physical units (meters) where appropriate.

- To obtain statistics for locations further downwind from the release point, we have included results for three more camera positions. One, camera B, at the same location as the original camera A, but with a smaller horizontal field of view, and similar cameras at about 300 m (camera B), and 500 m (camera C) downwind from the release point. For cameras B, C and D the release point of the plume is at a higher altitude to allow the cameras to see the full vertical extent of the plume. Furthermore, these cameras have more pixels in the vertical direction than camera A.

- To be able to compare the LES with the simulated images for these new camera viewing directions (viewing the plume at an elevation angle of 30.7° compared to 5.7°) new software had to be developed to calculate slant column densities along the camera lines of sight through the LES 3D concentration.

Below the comments from Referee #2 are given in italic font. Our responses to the comments are shown in roman font.

Specific comments

- *One criticism is that the usefulness of the fractal dimension calculation is unclear. Indeed, the authors description of the mass box counting method lacks detail, giving the impression that they do not know how best to make use of this parameter.*

  In response to the comment we have decided to leave this section out.

- *Another is that a more complete comparison could be made by comparing concentration PDFs. PDFs may or may not yield interesting information for the LES and simulated images used in this study, but in real turbulence one often finds intermittency, and its signature can be seen in the tails of the PDFs.*

  The images provides column densities (typically units of $1/\mathrm{m}^2$) along the line of sight of the camera. This is a quantity different from the concentration (units of $1/\mathrm{m}^3$) usually used to calculate PDFs. We have, however, calculated the probability density function (pdf) of the column densities from the LES and simulated images as shown in Fig. A1. These pdfs and their contribution to the explanation of the differences between the statitistical quantities from the LES and simulated images, are discussed in the revised manuscript.

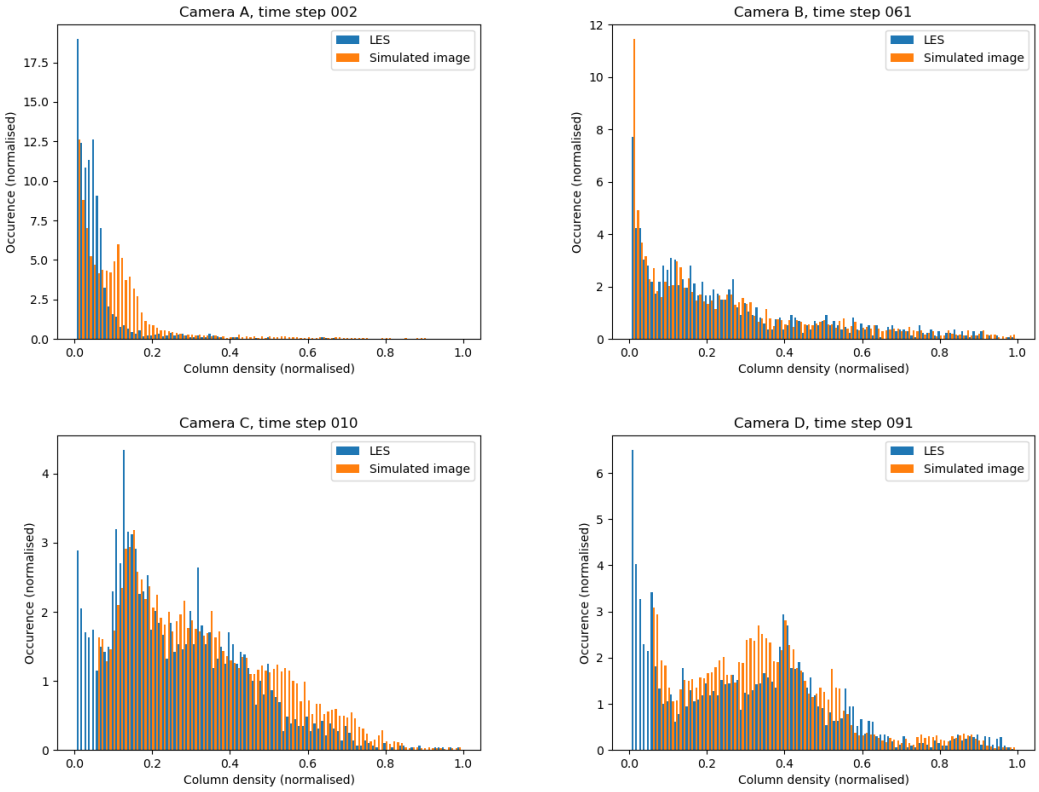

Figure A1: The probability density function (pdf) of the column densities from the LES and simulated images in Figs. 4-7 in the revised manuscript.

- *Finally, an analysis of the LES velocity field, projected onto the planes of the camera images (2D slices of the field), was not done. Calculations of divergence, vorticity and rate of strain in these 2D slices will help to identify vortex cores, saddle points and, where large 2D divergence will show up regions where out-of plane motion is significant. Such information will help interpret the structure of the concentration field and tracer dispersion, and the experience should generate intuition useful to the interpretation of images from real atmospheric flows.*

  A velocity field can be extracted from the camera images using for example the techniques described by Gliß et al. (2017). However, this velocity field is integrated by the concentration along the view path. As such it is very different from 2D slices and a comparison between the two is not trivial nor straightforward. The LES velocity and concentration fields are thoroughly discussed in the paper by Ardeshiri et al. (2020) which is cited in the manuscript.

Technical corrections

- *In the Introduction, please explain to the reader the motivation to investigate SO2 instead of some other tracer(s).*

To motivate the use of SO_2 we have added the following text to the Introduction:

> Over short transport distances, sulfur dioxide (SO_2) may be considered to be a passive tracer. Furthermore, SO_2 strongly absorbs radiation in part of the UV spectrum and may thus be detected by for example UV sensitive cameras (see for example Kern et al., 2010, and references therein).

- *Is this the first time a simulation of camera images or UV camera images have been attempted? If so, please say. If there have been previous efforts, were they successful or not?*

  To the authors knowledge UV camera images have not been simulated before. This statement has been added to the Introduction.

- *Page 2, line 17: The phrase "based on a large eddy simulation (LES)" does not convey the correct impression. I think you mean to say that you use LES in lieu of a real atmospheric flow.*

  We have rephrased this part so it now reads:

  > We present a novel method to simulate UV camera images of a dispersing SO_2 plume using a 3D radiative transfer model. The 3D descripton of the SO_2 plume is provided by large eddy simulation (LES) and are used in lieu of real atmospheric flow. The simulated images are used to examine how various factors (solar angles, aerosol content, and surface albedo) affect the statistical parameters characterizing the SO_2 plume dispersion.

- *The following sentence appears twice, once in the abstract and once in the conclusions. "Turbulence is one of the unsolved problems of physics." In both cases the sentence is unnecessary and distracting. It should be deleted.*

  This sentence has been removed both places as suggested.

- *A similar sentence appears in the Introduction (line 8): "The complete description of turbulence remains one of the unsolved problems of physics." This sentence also seems out of place and unnecessary and should be deleted.*

  The sentence has been removed as suggested.

Bibliography

Ardeshiri, H., Cassiani, M., Park, S., Stohl, A., I.Pisso, and Dinger, A.: On the convergence and capability of large eddy simulation for passive plumes concentration fluctuations in an infinite-Re neutral boundary layer, Boundary-Layer Meteorol., accepted for publication, 2020.

Gliß, J., Stebel, K., Kylling, A., Dinger, A. S., Sihler, H., and Aasmund, S.: Pyplis - A Python Software Toolbox for the Analysis of SO2 Camera Images for Emission Rate Retrievals from Point Sources, Geosciences, 7, https://doi.org/10.3390/geosciences7040134, URL `http://www.mdpi.com/2076-3263/7/4/134`, 2017.

Kern, C., Kick, F., Lübcke, P., Vogel, L., Wöhrbach, M., and Platt, U.: Theoretical description of functionality, applications, and limitations of SO_2 cameras for the remote sensing of volcanic plumes, Atmospheric Measurement Techniques, 3, 733–749, https://doi.org/10.5194/amt-3-733-2010, URL `http://www.atmos-meas-tech.net/3/733/2010/`, 2010.

Can statistics of turbulent tracer dispersion be inferred from camera observations of SO_2 in the ultraviolet? A modelling study

Arve Kylling[1], Hamidreza Ardeshiri[1], Massimo Cassiani[1], Anna Solvejg Dinger[1], Soon-Young Park[2], Ignacio Pisso[1], Norbert Schmidbauer[1], Kerstin Stebel[1], and Andreas Stohl[1]

[1]NILU - Norwegian Institute for Air Research, NO-2007 Kjeller, Norway
[2]Center for Earth and Environmental Modeling Studies, Gwangju Institute of Science and Technology, Gwangju, Republic of Korea

Correspondence to: Arve Kylling (arve.kylling@nilu.no)

Abstract. ~~Turbulence is one of the unsolved problems of physics.~~ Atmospheric turbulence and in particular its effect on tracer dispersion may be measured by cameras sensitive to the absorption of ultraviolet (UV) sun-light by sulfur dioxide (SO_2), a gas that can be considered a passive tracer over short transport distances. We present a method to simulate UV camera measurements of SO_2 with a 3D Monte Carlo radiative transfer model which takes input from a large eddy simulation (LES) of a SO_2 plume released from a point source. From the simulated images the apparent absorbance and various plume density statistics (centerline position, meandering, absolute and relative dispersion, ~~skewness, and fractal dimension~~and skewness) were calculated. These were compared with corresponding quantities obtained directly from the LES. Mean differences of centerline position, absolute and relative ~~dispersion~~dispersions, and skewness between the simulated images and the LES were generally found to be smaller than ~~a quarter of one camera pixel, with standard deviations between 1/2 and 3/2 camera pixel~~or about the voxel resolution of the LES. Furthermore sensitivity studies were made to quantify how changes in solar azimuth and zenith angles, aerosol loading (background and in plume), and surface albedo impact the UV camera image plume statistics. Changing the values of these parameters within realistic limits have negligible effect on the centerline position, meandering, absolute and relative dispersions, and skewness of the SO_2 plume. Thus, we demonstrate that UV camera images of SO_2 plumes may be used to derive plume statistics of relevance for the study of atmospheric turbulent dispersion.

1 Introduction

Air motion in the lowest part of the atmosphere is over land bounded by a solid surface of varying temperature and roughness. This part of the atmosphere is named the planetary boundary layer ~~(PBL) (Stull, 1988)~~(PBL, Stull, 1988). It responds quickly to surface radiation changes, and the air motion in the PBL is nearly always turbulent. A substance released into this turbulent atmosphere will~~experience concentration fluctuations~~ , at locations downwind of its source, experience concentration fluctuations that are important, particularly if responses are non-linear; for example with respect to toxicity, flammability and odour detection (e.g. Hilderman et al., 1999; Schauberger et al., 2012; Gant and Kelsey, 2012) and non-linear chemical reactions (Brown and Bilger, 1996; Vilà-Guerau de Arellano et al., 2004; Cassiani et al., 2013). The ~~complete description of turbulence remains one of the unsolved problems of physics. The~~ COMTESSA project (Camera Observation and Modelling of

4D Tracer Dispersion in the Atmosphere; https://comtessa-turbulence.net/) aims to "elevate the theory and simulation of turbulent tracer dispersion in the atmosphere to a new level by performing completely novel high-resolution 4D measurements". ~~To achieve this~~Over short transport distances, sulfur dioxide (SO_2) may be considered to be a passive tracer. Furthermore, SO_2 strongly absorbs radiation in part of the UV spectrum and may thus be detected by for example UV sensitive cameras (see for example Kern et al., 2010b, and references therein). Within COMTESSA, six UV cameras have been built to measure SO_2 densities from various viewing directions. A series of experiments with puff and continuous releases of SO_2 from a tower have been performed as described by Dinger et al. (2018). It is known from measurements of volcanic SO_2 emissions that aerosol and viewing geometry affect the retrieved SO_2 amounts (Kern et al., 2013). Furthermore, variations in surface albedo and solar zenith and azimuth angles may have an impact. The influence of these factors on the UV camera images, the deduced SO_2 amounts and density statistics needs to be quantified and, if necessary, corrected for.

~~The aims of this paper are to~~ Kern et al. (2013) performed radiative transfer simulations including a circular SO_2 plume, to estimate the effect of plume distance, SO_2 amount, and aerosol on the radiance at a UV camera location. However, to the authors knowledge, UV camera images have not been simulated before. We present a novel method to simulate UV camera images of a dispersing SO_2 plume ~~based on a~~ using a 3D radiative transfer model. The 3D descripton of the SO_2 plume is provided by large eddy simulation (LES) ~~of such a plume ; and~~ and are used in lieu of real atmospheric flow. The simulated images are used to examine how various factors (solar angles, aerosol content, and surface albedo) affect the statistical parameters characterizing the SO_2 plume dispersion. The large eddy simulation (LES) providing the input to the radiative transfer modelling, the radiative transfer model used to simulate the camera images and the statistical parameters are described in section 2. The effects of solar azimuth and zenith angles, surface albedo, background aerosol, and aerosols in the plume on plume density statistics are presented in section 3. Furthermore, the plume density statistics from the simulated images are compared with statistics derived directly from the LES simulations. The paper ends with the conclusions in section 4.

2 Methods

2.1 Large eddy simulation (LES)

Large eddy simulation is nowadays viewed as a popular tool in many applied atmospheric dispersion studies, especially of the urban environment and for critical applications such as the release of toxic gas substances (e.g. Fossum et al., 2012; Lateb et al., 2016). LES provides access to the three dimensional turbulent flow field and it is sometimes used as a replacement for experimental measurements at high Reynolds numbers. In this methodology, the large scales of the turbulent flow are explicitly simulated while a low-pass filter is applied to the governing equations to remove the small scales information from the numerical solution. The effects of the small scales are then parameterized by means of a sub-grid scale (SGS) model (e.g. Deardorff, 1973; Moeng, 1984; Pope, 2000; Celik et al., 2009). We used the Parallelized Large-Eddy Simulation Model (PALM, Raasch and Schröter, 2001; Maronga et al., 2015) to solve the filtered, incompressible Navier-Stokes equations in Boussinesq-approximated form, at infinite Reynolds number. A three dimensional domain of $1000\ \text{m} \times 375\ \text{m} \times 250\ \text{m}$ in the along wind (x), crosswind (y) and vertical (z) directions respectively, was simulated with a grid resolution of $nx \times ny \times nz =$

$1024 \times 384 \times 256$. Here nx, ny, nz are the number of grid nodes in along wind, crosswind and vertical directions, respectively. This implies that the size of a grid cell is $0.98^3\,\mathrm{m}^3 \approx 1\,\mathrm{m}^3$. The release point was located at ~~25~~ 25 and 150 m above the ground, depending on camera view direction, see section 2.2.

The neutral boundary layer was simulated as an incompressible half channel flow at an infinite Reynolds number. The flow was driven by a constant pressure gradient. For the velocity, periodic boundary conditions were used on the lateral boundaries while on the top, strictly symmetric, stress free, condition was applied. The bottom wall was not explicitly resolved but a constant flux layer was used as is commonly done in atmospheric simulations. Non-periodic boundary conditions were set for the passive scalar. For further information on the model set-up see also ~~?~~Ardeshiri et al. (2020).

The LES calculates 3D SO_2 concentrations as a function of time. The SO_2 concentrations are used as input to the 3D radiative transfer model simulations. A total of 100 time frames were calculated with a time resolution of 6.25 s. For the sensitivity studies one randomly chosen time frame was used, while seven and nine randomly chosen frames were used for the reference case ~~and the fractal dimension~~ calculation (see section 3). Both parts of the plume close to the release point and further downstream were used as input for the camera simulations. In Fig. 1 examples are provided of the part of the plume viewed by the different cameras (see section 2.2 for camera definition). Figs. 1a and 1b show the SO_2 column densities along the y and z-axes, respectively, for one instant of the LES simulation~~are shown along the y and z-axes in~~ . Fig. 1a shows approximately the part of the plume seen by camera A Figs. 1~~a and 1b, respectively, for~~ c and 1d show the part of the plume viewed by ~~the camera.~~ cameras B and C, respectively.

2.2 Radiative transfer simulations

The UV camera images were simulated with the 3D MYSTIC Monte Carlo radiative transfer model which was run within the libRadtran framework (Mayer et al., 2010; Emde et al., 2010; Buras and Mayer, 2011; Mayer and Kylling, 2005; Emde et al., 2016). MYSTIC includes an option to calculate the radiation impinging on a camera with a prescribed number of pixels in a plane defined by the location of the camera within a 3D domain and the camera viewing direction. For this option the MYSTIC Monte Carlo model is run in backward mode. The MYSTIC camera simulation capabilities have earlier been used by for example Kylling et al. (2013) to simulate infrared satellite images. Here it is used to simulate radiative transfer to ~~the~~ a UV camera at wavelengths suitable for the detection of SO_2. Thus, for each camera pixel, spectra were calculated for wavelengths ranging between 300 and 350.5 nm. The spectral resolution was 0.1 nm in order to capture the fine structure of the SO_2 cross section. The spectra were weighted with spectral response functions (about 10 nm width) representing cameras with mounted on-band (sensitive to SO_2 absorption, centred at 310 nm) and off-band (barely sensitive to SO_2 absorption, centred about 330 nm) filters similar to those described by Gliß et al. (2018). Quantum efficiency of the detector and geometrical effects related to lens/camera optics ~~are~~ were not included in the camera simulations. SO_2 plume concentrations were adopted from the LES simulations described in section 2.1 and the spectrally dependent SO_2 absorption cross section was taken from Hermans et al. (2009).

A finite 3D domain (bird's eye view provided in Fig. 2) is defined for the radiative transfer simulations. The SO_2 plume is embedded in this domain and is viewed from the side at a distance of about 250 m by the UV camera, which is placed

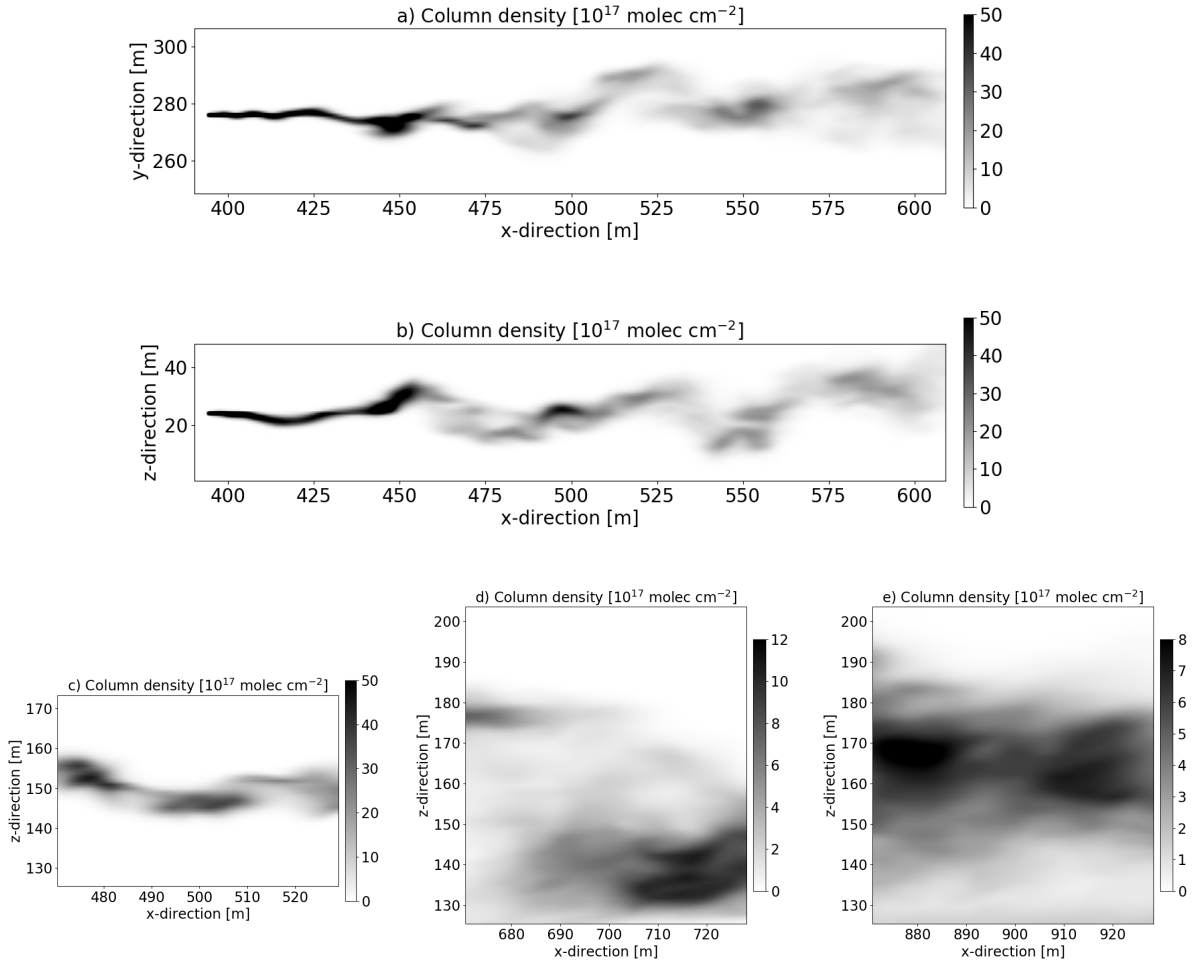

Figure 1. a) SO_2 column densities from the LES (time frame no. ~~5~~2) integrated along the vertical z-direction. This corresponds to the part of the plume viewed by camera A. b) Corresponding SO_2 column densities integrated along the cross-wind y-direction. c-e) LES SO_2 column densities (time frames no. 61, 10 and 91) integrated along the cross-wind y-direction, corresponding to the part of the plume viewed by cameras B, C and D respectively. Note the different scales of the grayscale bars.

1~~meter~~ m above the surface. This camera-plume distance is comparable to that used during part of the first COMTESSA field campaign described by Dinger et al. (2018).

~~As the COMTESSA field campaigns are being carried out primarily in central Norway during the summer time, solar zenith angles of 40° and 60° were considered. When not otherwise noted (see section 3.2), the sun was assumed to be perpendicular to the camera viewing direction, see Fig. 2~~Four different cameras at different locations and viewing geometries were simulated. These are summarized in Table 1. Camera A captures the plume from its release point and about 200 m downwind. It sees the

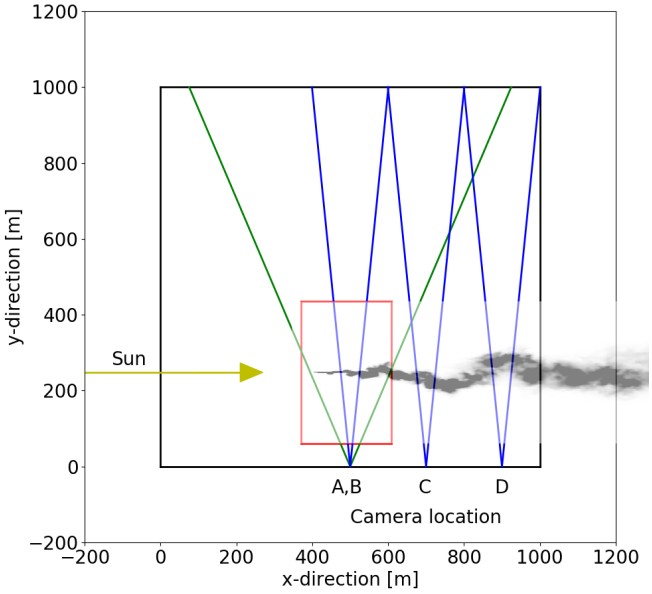

Figure 2. Bird's eyes view of the 3D domain (black square) and the SO_2 plume location within the domain (red square for camera A simulation, shifted along x-axis for the other cameras). The UV ~~camera is~~ cameras are located where the two green or blue lines intersect. ~~They~~ The lines indicate the ~~camera's~~ horizontal field-of-view of the cameras whose location is given in Table 1. The column density (similar to the upper plot in Fig. 1) of the plume is included for illustrative purpose. The direction of the incoming Sun ray is shown by the yellow line.

Table 1. Location and geometric specification of the three simulated cameras. All cameras were placed 1 meter above the surface.

Camera	FOV (degrees)	Viewing elevation (degrees)	No. of pixels. (horizontal×vertical)	x-location (m)
A	46°×10°	5.73°	400×88	500
B	11.5°×30°	30.7°	100×264	500
C	11.5°×30°	30.7°	100×264	700
D	11.5°×30°	30.7°	100×264	900

plume released at an altitude of 25 m and thus have a low angle viewing elevation, see Table 1. Cameras B, C and D resembles a different experimental situtation with the plume release altitude of 150 m. These cameras thus have a larger viewing elevation. Camera A is placed at the same x-direction location as camera A, but as a smaller horizontal FOV to focus on the more mature

parts of the plume. Cameras C and D are placed further downwind and views the plume about 300 and 500 m downwind from the release point, respectively.

The LES voxel resolution is about 1 m^3 which at a distance of 250 m corresponds to 0.004 rad=0.23°. ~~The simulated camera field of view (FOV) was set to 46°×10° to cover the main plume.~~ To ensure sufficient spatial sampling the camera resolution was specified to be about half the LES voxel resolution. ~~With the FOV and~~ To be able to see the plume at the various camera position the camera field of view (FOV) was varied and the number of pixels adopted to give a camera resolution of about 0.5 m at the plume~~, this gives a camera with 400×88 pixels~~. It is noted that the UV cameras used by Dinger et al. (2018) had 1392×1040 pixels. The reason and justification for using fewer pixels in the simulated camera are twofold: 1) With the simulated camera it is possible to zoom onto the plume as one always knows where the plume is. In an experimental setting, the plume usually covers only part of the FOV, to allow for changes in wind direction and, thus, changes in plume position; 2) The computer time and memory requirements increase as the number of pixels increases. It is thus advantageous to use as few pixels as needed to cover the plume.

As the COMTESSA field campaigns are being carried out primarily in central Norway during the summer time, solar zenith angles of 40° and 60° were considered. When not otherwise noted (see section 3.2), the sun was assumed to be perpendicular to the camera viewing direction, see Fig. 2.

To further save computer memory and time, a full 3D description of the plume is given only in the part of the domain containing the plume seen by the camera (red square in Fig. 2). Outside the red square, the plume is not included. Energy conservation is ensured by using circular boundary conditions, that is, photons leaving the domain on one side enter the domain again on the opposite side. This implies that the plume may be seen several times by the camera if not enough care is taken when setting up the geometry of the computational domain, the location of the plume within the domain, and the camera. ~~This is challenging in the present situation where a realistic experimental setup is simulated~~ For camera A this is challenging (low altitude plume, camera viewing angles close to the horizon). Great care was thus taken when setting the domain size and the camera A field of view to avoid "ghost" plumes in the simulated images. Still, part of a secondary "ghost" plume is present in some of the images. These "ghost" plumes have been removed from the analysis presented below for camera A.

For representing the ambient atmosphere the mid-latitude summer atmosphere of Anderson et al. (1986) was used. The surface albedo is small in the UV for non-snow covered surfaces and was thus set to zero when not otherwise noted (see section 3.4). Aerosols were included for specific sensitivity tests that are described in section 3.3.

The radiative transfer simulations were run on a Linux cluster utilizing 10 processors in parallel with each process needing about 10-15 GB of memory depending on whether aerosols in the plume were included or not. The MYSTIC Monte Carlo radiative transfer simulation is statistical in nature and the simulated images thus contain statistical noise. To achieve a noise level of about the same order of magnitude as the measurements ($\approx 1\%$), a sufficient number of photons needs to be traced. For each pixel and wavelength 2000 photons were traced. This gave simulation times for one on- and one off-band image of about 120-140 hours, and ensured that for the simulations without aerosol and zero surface albedo at least 93.0% of the pixels had radiances with a relative standard deviation $<1.0\%$. For simulations with background aerosols the corresponding number is 83%.

2.3 Analysis methodology

The apparent absorbance for the on-band camera is given by Mori and Burton (2006) and Lübcke et al. (2013)

$$\tau_{on} = -\ln \frac{I_{on,M}}{I_{on,0}} \tag{1}$$

Here, $I_{on,M}$ is the on-band radiance and $I_{on,0}$ the background radiance without the SO_2 plume. In addition to absorption by SO_2, τ_{on} may include absorption due to aerosol and plume condensation. Assuming that the absorption by these other constituents varies little with wavelength between the on- and off-band cameras, the extra absorption may be removed by subtracting the off-band absorption:

$$\tau = \tau_{on} - \tau_{off} = -\ln \frac{I_{on,M}}{I_{on,0}} + \ln \frac{I_{off,M}}{I_{off,0}} = \ln \left(\frac{I_{off,M}}{I_{on,M}} \frac{I_{on,0}}{I_{off,0}} \right), \tag{2}$$

where $I_{off,M}$ and $I_{off,0}$ are the off-band radiance and the off-band background radiance respectively. The background images were calculated similar to the plume images, but with the SO_2 concentration set to zero. Below, plume statistics are presented for both τ_{on} and τ.

Ideally, plume statistics from the LES SO_2 concentrations and image derived SO_2 concentrations should be compared. However, for the images this would require simulating a geometry suitable for tomography and tomographic reconstruction of the plume. The slant column density (SCD) is the concentration of a gas along the light path (typically in units of m^{-2}). It ~~may be readily~~ is calculated from the LES SO_2 concentrations by tracing individual rays corresponding to individual camera pixels. From apparent absorbances the SCD may be retrieved. For SO_2 camera measurement this is done by calibrating the camera with SO_2 cells and/or concurrent differential optical absorption spectroscopy (DOAS) measurements. The calibration gives a linear relationship between the apparent absorbance and the SCD (see for example Lübcke et al., 2013). Such calibration procedures could be simulated and used to calibrate the simulated images. However, higher order moments (first order moment and upwards) would be the same for the SCD and the apparent absorbance due to the linear relationship between the two. Thus, below we will compare SO_2 SCD from the LES with apparent absorbance from the images. We note that this comparison will not include the zeroth moment (total mass) and that systematic biases may go undetected. While a comparison of the total mass certainly is of interest, this would require a systematic investigation of SO_2 calibration using simulated images, which is beyond the scope of this work.

2.3.1 Plume statistics

For projected LES simulations and the simulated images, the vertical (in the images) plume centerline position, meandering, absolute and relative dispersions, and the skewness were calculated (see e.g. Dosio and de Arellano, 2006). However, the absolute dispersion can only be properly defined using an ensemble or time average. As this is not possible here due to the above mentioned computing limitations, we use the center of the source ($\overline{z} = z_0$) as the reference vertical position.

Each pixel in the camera images and each projection from the LES simulations describe the integrated column amount (ρ_L) of the trace gas along the line of sight (dL):

$$\rho_L = \int \rho dL \tag{3}$$

where ρ is the density of the trace gas. The ~~mean plume height $\overline{z}$ and the~~ instantaneous vertical plume centerline position ~~$\overline{z_m}$ are~~ z_m is given by

$$= \frac{\iint z \rho_L dx dz}{\iint \rho_L dx dz} z_m(x) = \frac{\int z \rho_L dz}{\int \rho_L dz} \tag{4}$$

where ~~z is the pixel number in the vertical direction and x is the pixel number in the horizontal direction. We note that strictly speaking world coordinates should be used instead of pixel numbers in the equations above and below. However, for the geometry in this study the difference between the two is less than 1%. Thus, for convenience we use pixelnumbers~~and z are the horizontal and vertical positions of the pixel, respectively.

~~Following Dosio and de Arellano (2006) we define the~~ The fluctuations of the absolute, relative and centerline positions ~~:~~ are defined as

$$z' = z - z - z_0 \tag{5}$$

$$z_r = z - z_m \tag{6}$$

$$z'_m = z_m - z_0. \tag{7}$$

~~Ideally, some time-averaged value of $\overline{(z)}$ should be used in Eqs. 5-7. Here we calculate $\overline{(z)}$ from a single time step. This implies that~~ It is noted, that with this definition of the absolute position, relative and absolute dispersion are the same at the source location, since meandering here is zero. Also, since we set $\overline{z} = z_0$, there will be correlations between z'_m at different x, which also implies that $\overline{(z'_m)}$ is strictly speaking not a robust reference for defining meandering of the plume. However, the purpose of this study is to investigate the sensitivity of the statistical properties to changes in various atmospheric parameters and this limitation should have minimal impact on the results.

The absolute (σ_z), relative (σ_{zr}) and meandering (σ_{zm}) dispersions are defined as:

$$\sigma_z^2(x) = \frac{\int \rho_L z'^2 dz}{\int \rho_L dz} \tag{8}$$

$$\sigma_{zr}^2(x) = \frac{\int \rho_L z_r^2 dz}{\int \rho_L dz} \tag{9}$$

$$\sigma_{zm}^2 = \frac{\int \rho_L z_m'^2 dx}{\int \rho_L dx} \tag{10}$$

and similarly for the skewnesses:

$$\overline{z'^3} = \frac{1}{\sigma_z^3(x)} \frac{\int \rho_L z'^3 dz}{\int \rho_L dz} \tag{11}$$

$$\overline{z_{zr}'^3} = \frac{1}{\sigma_{zr}^3(x)} \frac{\int \rho_L z_r^3 dz}{\int \rho_L dz} \tag{12}$$

$$\overline{z_{zm}'^3} = \frac{1}{\sigma_{zr}^3(x)} \frac{\int \rho_L z_m'^3 dx}{\int \rho_L dx} \tag{13}$$

These various quantities were calculated both directly from the projected LES simulations and also from the camera images. The former served as a reference ("ground truth") against which the quantities derived from the camera images were compared.

2.3.2 Fractal dimension

Turbulent flow is non-uniform. Thus, besides describing the flow with various moments as explained in section 2.3.1, it may be fruitful to use fractal methods to analyse tracer dispersion. One method for determining the fractal dimension is the box-counting algorithm. The box counting dimension, D_{box}, or Minkowski-Bouligand dimension, is defined as (see for example Feder, 198

$$D_{\text{box}} := \lim_{\epsilon \to 0} \frac{\log(N(\epsilon))}{\log(1/\epsilon)}.$$

Here ϵ is the side length of the boxes used to measure the number of boxes $N(\epsilon)$ covering the feature of interest. Here we define the feature of interest to be the SO_2 plume where the apparent absorbance $\tau > 0.03$, see Eq. 2 and Fig. 3. The threshold on τ is set in order to avoid influence from noisy pixels. From the threshold filtered and gray-scaled τ-images the fractal dimension was estimated using the mass box counting method. This was done both for projected LES simulations and simulated UV camera images. The Fractal Dimension and Lacunarity (FracLac) plugin to the Image processing and analysis in Java (ImageJ) software (Karperien, 1999-2013; Rasband, 1997-2018), was used to calculate the fractal dimension.

3 Results

We first compare statistical results from the LES and simulated images reference atmospheric conditions. This comparison is made for both single and multiple time frames and is done in order to estimate how well the camera derived statistics may reproduce the LES statistics. Next the impact of solar angles, aerosol load, and surface albedo on plume statistics are investigated for a single time frame.

3.1 Reference cases

Figs. 3a and 3b show simulated on- and off-band radiances, respectively, for camera A and the reference case (no aerosol, zero surface albedo and a solar zenith angle of 40°). The strong absorption of SO_2 in the on-band image is clearly visible in Fig. 3a. There is also a weak SO_2 signal in the off-band image (Fig. 3b). From the on- and off-band images, and corresponding background images not including the SO_2 plume, the apparent absorbance was calculated using Eq. 2. The resulting apparent absorbance is shown in Fig. 3c on a linear scale and in Fig. 3d on a logarithmic scale.

The apparent absorbance is reproduced in Fig. 4a, while Fig. 4b shows the SCD calculated along the line of sights using the LES concentrations. The plume centerline, absolute and relative dispersiondispersions, and skewness, as defined in Eqs. 4, 8 and 11, were calculated directly from the LES density values in Fig. 1from the simulated images and the LES images. These are shown as solid lines in Fig(LES) and dotted lines (camera simulation) in Figs. 4. The same quantities were derived from the apparent absorbance in Fig. 3 and are shown as dotted lines in Fig. 4 for comparison. (a) The plume apparent absorbance from Fig. 3c with the centerline overlaid in red. (b) The absolute and relative dispersions (note $\log_{10}$ axes). (c) The skewness. Solid lines are calculated directly from the LES densities and shifted to the camera pixels, while dotted lines are derived from the

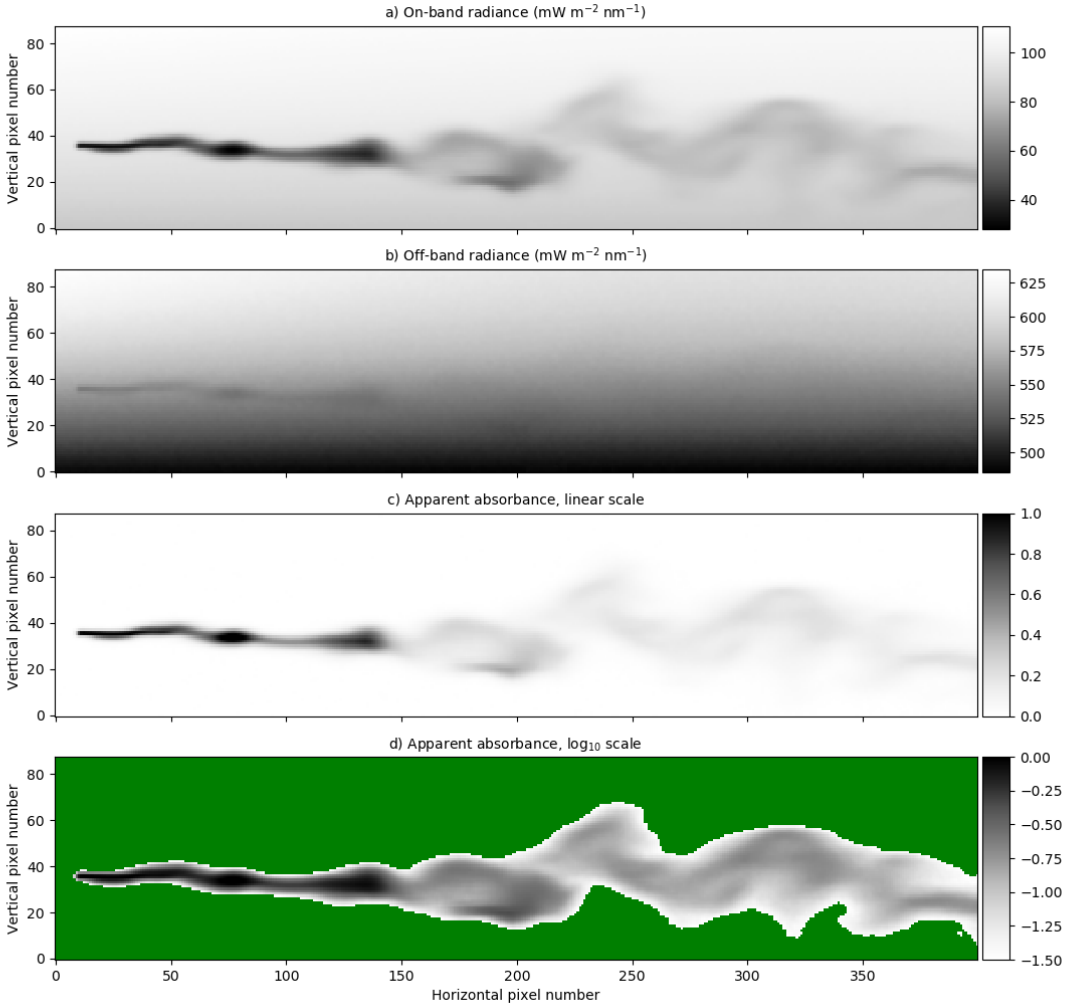

Figure 3. Radiances and apparent absorbance for ~~the~~ camera A , same time frame as in Fig. 1. (a) The on-band radiance. (b) The off-band radiance. (c) The apparent absorbance calculated using Eq. 2. (d) Same as (c) but with logarithmic grey scale. The green colour represents pixels for which the apparent absorbance $\tau < 0.03$.

~~simulated images. Note that the x-axis scales in panels a) and c), while in different units, are the same.~~ ~~The centerlines (Fig~~a and b. Similar plots for cameras B, C and D are presented in Figs. 5-7. Note that the simulated and LES images in Figs. 4~~a) and the skewnesses (~~-7 differs from those in Fig. ~~4c) are shown as linear functions of horizontal pixel number. The absolute and relative dispersions (Fig. 4b) are shown on a log$_{10}$-log$_{10}$ scale.~~ 1 due to different viewing directions. In the latter the plumes are viewed at an viewing angle of 0° while for cameras A, B, C and D the viewing angle differs from the horizontal, see Table 1.

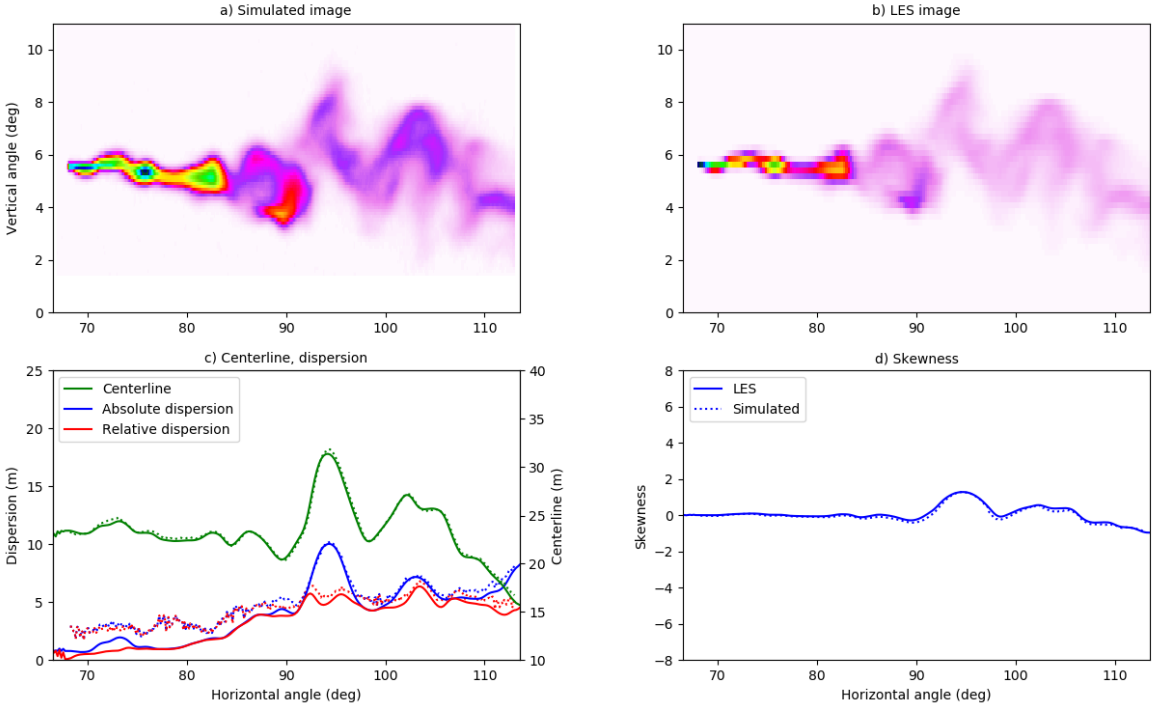

Figure 4. a) The plume apparent absorbance from Fig. 3c. b) The LES column density integrated along the line of sight. Colorscales in a) and b) are relative and thus no colorbars are provided. c) The centerline, absolute and relative dispersions. d) The skewness.

Overall the behaviour of the centerline, absolute and relative dispersions and skewness calculated from the simulated images is similar to those from the LES densities ~~. The altitude of the centerline is slightly underestimated for horizontal pixels (viewing angles) larger than about 330 (15°) . Furthermore the skewness from the simulated images differs for horizontal viewing angles <0°.The relative and absolute plume dispersion derived from the calculated images is generally~~ for all cameras. The centerlines agrees well for all four cameras. For camera A, Fig. 5, the absolute and relative dispersions from the camera are larger than those from the LES for the plume downwind to about 100 m (corresponding to $\approx 90°$ horisontal viewing angle) from the release point. For camera B, Fig. 5, all quantities agree well, while for cameras C (Fig. 6) and D (Fig. 7), the camera dispersions are larger than the ~~corresponding LES-values for pixels less than about 100. However, notice that in particular the relative dispersion is smaller than one pixel close to the source, and thus it is highly sensitive to even small~~ LES dispersions by about 50-60% and the magnitude of the skewness from the camera is also larger.

To shed further light on the differences between the ~~simulated images~~ images from the radiative transfer simulation and the LES ~~concentrations. The MYSTIC Monte Carlo simulations add some noise and thus the dispersion is expected to be larger when derived from the simulated images. For~~ we show the probability density function (pdf) of the column densities from the LES and simulated images in Fig. 8. These pdfs represent area sample pdfs and cover the full images. For camera A the pdfs

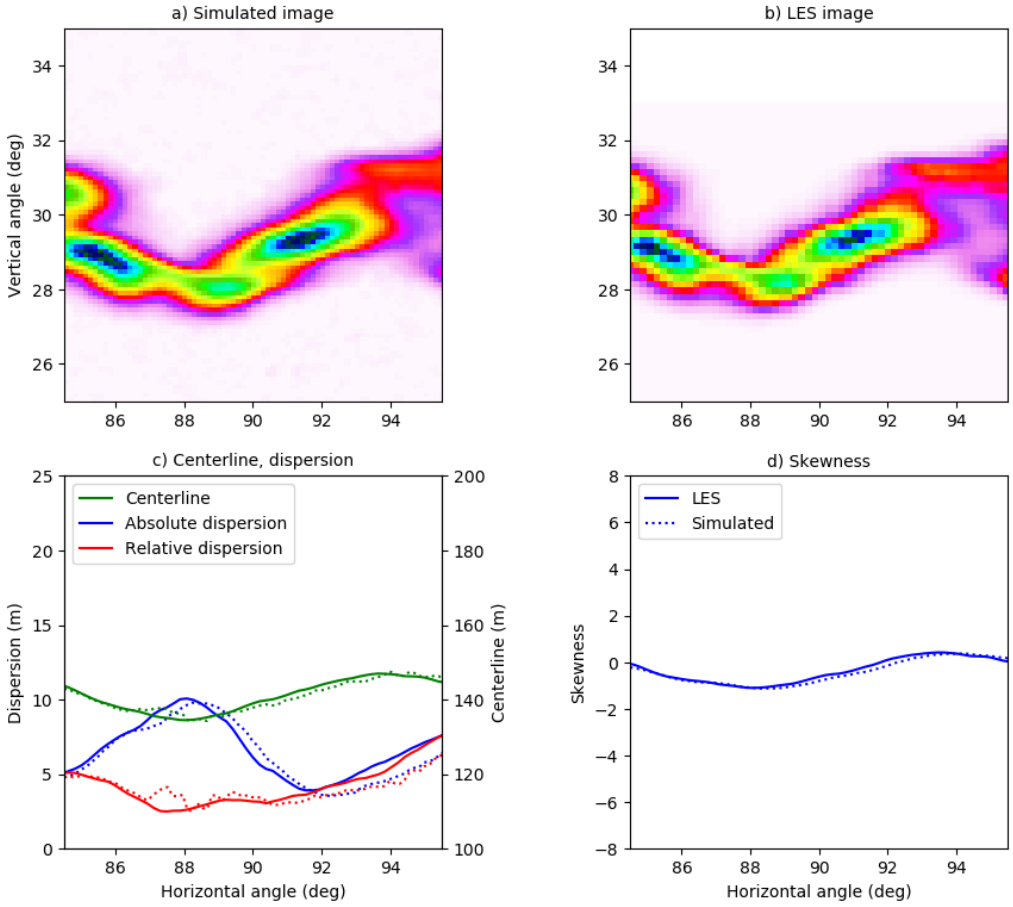

Figure 5. Similar to Fig. 4, but for camera B and time step 61.

differ for intermediate values, where an artificial secondary peak is created in the pdf for the simulated image. This is most likely due to the diffusive nature of the radiative transfer in the young part of the ~~denser part of the plume the absorption of radiation by SO_2 may be saturated (the maximum apparent absorbance is about 1.0) , and thus decreasing the skewness~~plume (horizontal angle smaller than about 85°) where the LES plume is of the size a few voxels. However, ~~inspection of the differences of the third moments without disperion normalization, shows that the differences in skewness is in part driven by the differences in the dispersion. In general, the differences are small and less than one pixel for the entire FOV.~~

~~During the COMTESSA campaigns both continuous and puff releases of SO~~the SO_2 ~~are done.For puffs the dispersion increases as the square of the time, t^2, of flight (see Dinger et al., 2018, and references therein). Taking the horizontal pixel number as a surrogate for time (Taylor's frozen turbulence hypothesis) we note the linear behaviour of the relative dispersion for pixels close to the release point (Fig. 4b). A linear fit for pixels between 10 and 30 gives slopes of 0.0100 and 0.0217 for~~

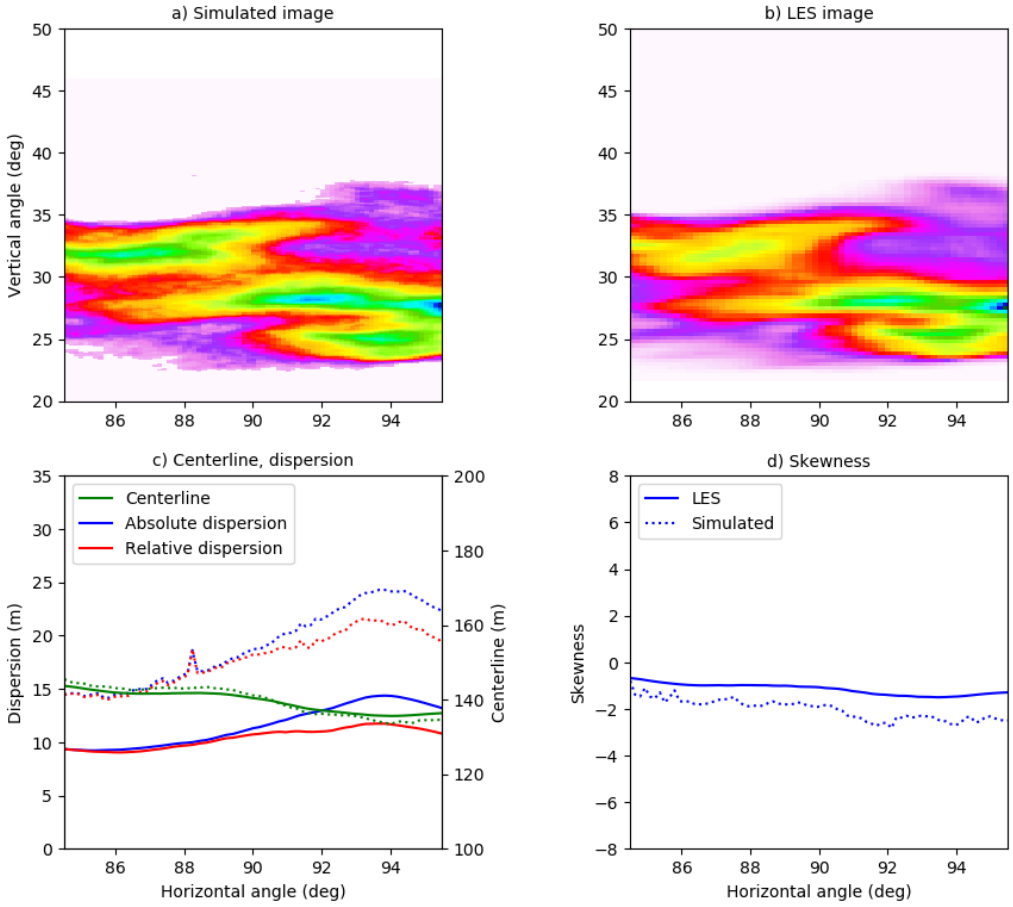

Figure 6. Similar to Fig. 4, but for camera C and time step 10.

~~the relative dispersion derived from the simulated images and~~ absorption signal is strong and thus the centerline, dispersions and skewness agree well for the dispersed part of the plume. For camera B the pdfs are similar and this is reflected in the good agreement between the statistical quantities presented in Fig. 5. This indicates that the when the plume is large enough compared to the pixel resolution the camera can capture the plume well . The pdfs for camera C exhibit much the same behaviour. However, at this further downwind location, the plume is more dispersed, the SO_2 absorption signal weaker and sometime beyond detection (thus the lower cut-off in the pdf of the simulated image). The weaker absorption signal implies that the ~~LES concentrations. If the fit region is changed to pixels between 40 and 60 the slopes changes to 0.0170 and 0.0159 respectively. The results also vary with fit region for other time steps. The relative dispersion is less than one pixel for horizontal pixel numbers smaller than about 60. The differences in slope when varying the fit region suggest that for the t^2 expansion regime care must be taken when the magnitude of the relative dispersion is small (less than about one pixel)~~ statistical noise

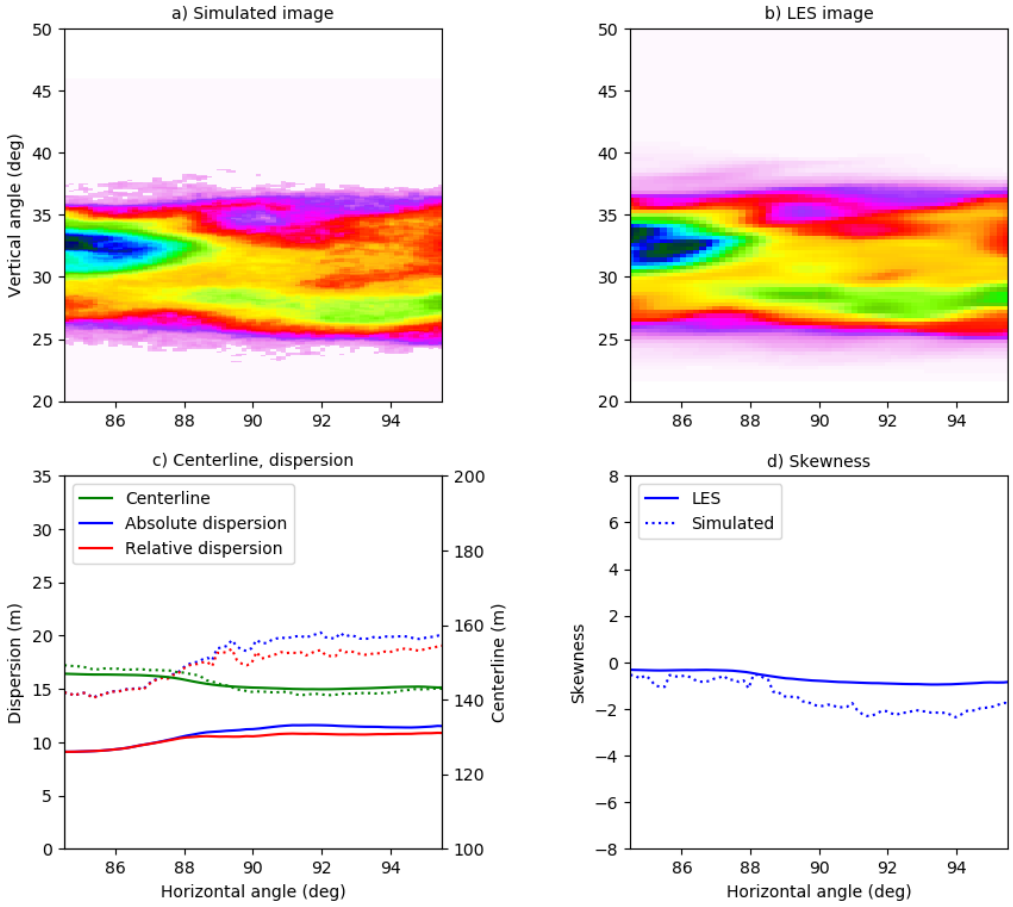

Figure 7. Similar to Fig. 4, but for camera D and time step 91.

from the Monte Carlo based radiative transfer simulation becomes discernible and increases the dispersions compared to the ~~pixel size of the camera.~~ LES, Fig. 6. A similar situation is evident for camera D, see pdfs in Fig. 8 and statistical quantities in Fig. 7

As noted above, a large number of images such as in Fig. 3 is required to estimate the parameters of interest for description of turbulence. This is not computationally feasible with available resources. However, ~~to~~ it is noted that if the instantaneous statistics are correct, the ensemble statistics will also be correct. This is not necessarily true the other way around. To provide an estimate of the difference between the statistical quantities from the simulated images and the LES densities, the differences between the centerline, the absolute and relative dispersions and the skewness, were calculated for seven (camera A) and nine (cameras B, C and D) random time steps. The mean differences and the standard deviations are summarized in Table 2. The mean differences between the quantities from the simulated images and the LES densities are ~~on the sub-pixel level.~~

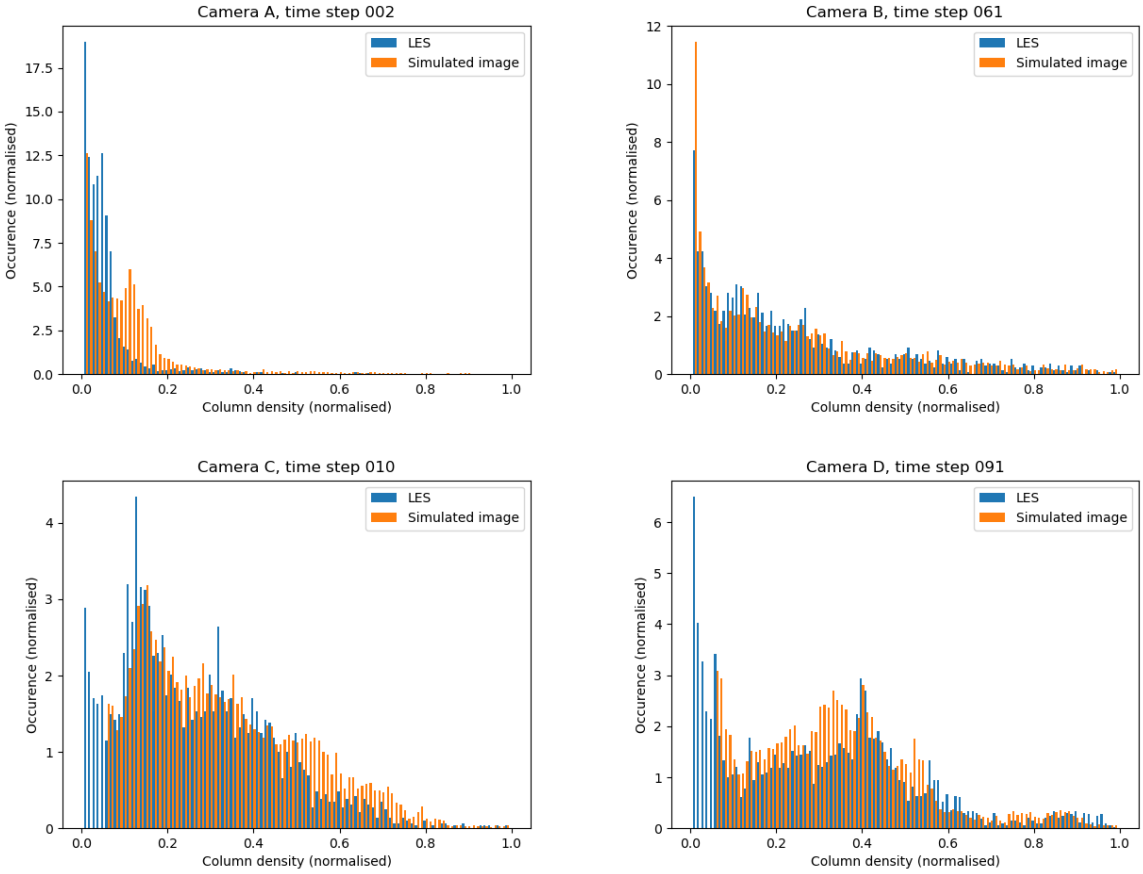

Figure 8. The probability density function (pdf) of the column densities from the LES and simulated images in Figs. 4-7.

Table 2. The mean±the standard deviation for the difference between the simulated images and the LES densities for ~~the time frame shown Fig. 3, and for seven time randomly chosen steps. Numbers are in units of pixels.~~seven (camera A) and nine (cameras B, C and D) randomly chosen time steps.

Camera	Timestep(s)	Centerline ~~Dispersion~~ (m)	Absolute ~~Dispersion~~ dispersion (m)	Relative dispersion (m)	
A	5, 13, 22, 31, 41, 60, 97	~~0.857~~0.060±~~1.372~~ 0.203	~~-0.152~~0.955±~~1.541~~ 0.655	~~-0.210~~1.243±~~1.338~~ 0.602	~~0.~~
~~5, 13, 22, 31, 41~~B	7, 23, 32, 48, 60, 61, 65, 75 91	-0.503±1.164	-1.088±1.612	-0.240±0.565	
C	7, 23, 32, 48, 60, ~~97~~ 61, 65, 75 91	~~0.521~~-1.069±~~1.581~~ 2.582	~~0.321~~4.989±~~1.346~~ 2.141	~~0.047~~4.429±~~0.870~~ 2.030	~~0.~~
D	7, 23, 32, 48, 60, 61, 65, 75 91	-0.353±2.851	7.658±1.839	7.036±1.681	

~~However, the standard deviations of the differences are larger. Possible sources~~ small for cameras A and B. For the centerline and the dispersions the differences are about or smaller than the voxel resolution of the LES simulations. For camera C the centerline differences are about the LES voxel resolution, whereas the dispersion differences increase. Camera D differences shows similar behaviour, but with even larger differences for the dispersions. As already mentioned above, the main source for the differences ~~include~~ is the Monte Carlo noise in the radiative transfer ~~simulations, image sampling resolution, and errors caused by the spatial resolution of the LESdensity~~simulation when the SO_2 signal becomes weak. This alters the dispersions, Figs. 4-7 and pdfs, Fig. 8. This is evident in the simulated images dispersions, which are not as smooth as those from the LES, Figs. 5-.7. It must also be emphasized that the densities simulated by ~~LES and~~ the LES and the apparent absorbance are not the same physical quantities, but are non-linearly connected through the radiative transfer equation. ~~However, the generally small differences in statistical quantities derived directly from the LES and the radiative transfer model show that apparent absorbance can well serve as a proxy for light-path-integrated density with respect to characterizing turbulent dispersion.~~

3.2 Solar azimuth and zenith angle effects

In Figs. 3 and 4 results were shown for solar azimuth and zenith angles of $\phi_0 = 90°$ and $\theta_0 = 40°$, respectively. The simulations were repeated for a solar zenith angle of $\theta_0 = 60°$ to see if this would change the plume statistics. The difference in apparent absorbance, $\delta\tau = \tau(\theta_0 = 60) - \tau(\theta_0 = 40)$, is shown in Fig. 9. The apparent absorbance is generally slightly smaller (on

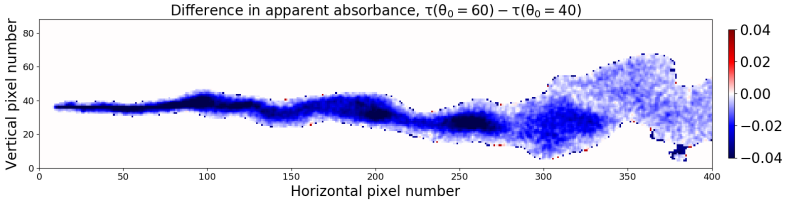

Figure 9. The difference in apparent absorbance from images recorded at two different solar zenith angles, $\theta_0 = 60°$ and $\theta_0 = 40°$.

average about 6%) for $\theta_0 = 60°$ than for $\theta_0 = 40°$. Ideally the apparent absorbance is due to photons travelling along a straight lines passing through the plume and into the camera. However, photons taking other paths may also contribute to the signal. Direct solar radiation photons contribute in three ways to the camera signal through: 1) direct photons scattered behind the plume in the direction of the camera; 2) direct photons scattered in the plume towards the camera; and 3) direct photons scattered between the plume and the camera in the direction of the camera. The first part is included in the apparent absorbance and does not depend on solar zenith angle due to the background correction. The third part is called light dilution and does not depend on the amount of SO_2 in the plume. The second part depends on the amount of SO_2 in the plume and the solar zenith angle. The latter because there is relatively more direct radiation at $\theta_0 = 40°$ than at $\theta_0 = 60°$. Hence, more direct radiation is likely to enter the plume for $\theta_0 = 40°$ and being scattered into the camera from inside the SO_2 plume. This explains the

negative difference in the apparent absorbance between $\theta_0 = 60°$ and $\theta_0 = 40°$. It is noted that in an experimental setting, where calibrations are carried out throughout the day, solar zenith angle variations will not neccessarily give a change in SO_2.

Statistics were calculated as ~~in Fig. 4~~ for the $\theta_0 = 40°$ case and differences to this case are summarized in Table 3, rows labeled "$\theta_0 = 60°$". In the table, differences are reported as the maximum difference in units of ~~pixel and the percentage of difference values that were larger than one pixel.~~ meters. Differences are reported both without and with the off-band correction, Eqs. 1 and 2 respectively, to quantify the impact of the correction. Overall, the statistics for the $\theta_0 = 60°$ results deviate little from the $\theta_0 = 40°$ case~~, except for the absolute dispersion, for which 2% of the values differed by more than one pixel.~~ . The difference in meandering, not shown in Table 3, is negligible for this and all sensitivity cases below, and is not further discussed.

The sensitivity to the solar azimuth angle was investigated by setting the solar azimuth angle to $\phi_0 = 0, 45, 135, 180,$ and $270°$, while keeping the solar zenith angle at $\theta_0 = 40°$. The difference in absorbance is less than 0.05% on average. The impact on the centerline, absolute and relative dispersions and skewness is negligible, see rows labeled "$\phi_0 = 0 - 270°$" in Table 3. From the results no preferable solar azimuth-camera viewing direction geometry may be identified. However, note that the azimuth angle of the background image needs to be the same as for the image with SO_2. ~~As no aerosols are included in theses simulations, the differences with and without off-band correction are similar. Finally it~~ It is noted that including aerosols has negligible effect on the solar azimuth angle sensitivity, see section 3.3.

3.3 Aerosol effects

No aerosols were included in the simulations above. Background aerosols may be present in both the plume and in the surrounding atmosphere. Furthermore, aerosol may be present in the plume due to formation of sulfate aerosol from SO_2. Both cases are investigated below.

First, background aerosol with an optical depth $t_{BG}(310) = 0.5$ and a single scattering albedo (SSA) of about 0.95 at 310 nm, were included in simulations for $\theta_0 = 40°$ (The aerosol_default option of uvspec was used, see Emde et al., 2016). The difference between the simulation including background aerosol and the aerosol free simulation is shown in Fig. 10a. Including background aerosol gives generally a slightly lower apparent absorbance, on average about 2.5% whether the off-band correction is excluded or included, Eqs. 1 and 2 respectively. The decrease is due to multiple scattering by the aerosol and hence less direct radiation (Kern et al., 2010a). The background aerosol had negligible effect on plume statistics, Table 3, rows labeled “BG aerosol”.

Simulations were also made with aerosol in the plume only, that is various amounts of aerosol were added to the voxels containing SO_2. This is relevant for non-pure SO_2 plumes where aerosols are co-emitted such as from power plants, or where secondary sulfate aerosols may form in the SO_2 plume. The impact of both highly absorbing (SSA=0.8) and purely scattering aerosol (SSA=1.0) were investigated. Kern et al. (2013) concluded that if a plume contains an absorbing aerosol component the retrieved SO_2 columns may be underestimated. Here we estimate the effect of aerosols in the plume on the higher order statistics of the plume. Figs. 10b and 10c show the difference in apparent absorbance between simulations with and without absorbing aerosol in the plume for a relatively large aerosol optical depth of about 0.5 (Fig. 10b) and an unrealistic extreme case with aerosol optical depth of about 5.0 at 310 nm (Fig. 10c). Results for non-absorbing aerosol are similar (not shown).

Table 3. Summary of differences in statistics between the baseline case shown in Fig. 4 and the sensitivity tests (first column). The second column reports the mean and standard deviation (std) of the difference in absorbance ($\delta\tau$). For the centerline, absolute dispersion ~~, relative dispersionand skewness~~and relative dispersion, the mean and standard deviation (std) are given in units of ~~pixels, together with the percentage of pixels where the differences are larger than one pixel (columns labeled %)~~meters. For the azimuth dependence sensitivity, tests were made for a range of angles, the numbers in the table are the extreme values for all these tests.

Sensitivity test	$\delta\tau$ Mean±std	Centerline Mean±std	Absolute dispersion ~~%~~ Mean±std	Rela dispe ~~%~~ Mea
		Including off-band correction, Eq.2.		
$\theta_0 = 60°$	-0.0097±0.0130	~~0.0151~~-0.0071±~~0.1693 0.8~~0.0830	~~0.0545~~0.0150±~~0.2216 1.8~~0.0740	~~0.0580~~0.0211±~~0.~~
$\phi_0 = 0 - 270°$	-0.0005±~~0.0001±0.0029~~0.0033	~~-0.0048~~-0.0042±~~0.1213 0.3~~0.0498	~~-0.0079~~-0.0064±~~0.12440.3~~0.0900	~~-0.0098~~-0.0086±~~0~~
BG aerosol	-0.0044±0.0089	~~-0.0143~~0.0071±~~0.1597 0.5~~0.0791	~~-0.0111~~-0.0066±~~0.0848 0.0~~0.0565	~~-0.0199~~-0.0111±~~0~~
$\tau_{plume} \sim 0.5$, ssa=0.8	-0.0003±0.0025	~~-0.0006~~0.0002±~~0.0832 0.0~~0.0412	~~-0.0030~~-0.0036±~~0.0853 0.3~~0.0477	~~-0.0023~~-0.0028±~~0~~
$\tau_{plume} \sim 0.5$, ssa=1.0	-0.0003±0.0024	~~-0.0070~~0.0034±~~0.0918 0.3~~0.0451	~~-0.0079~~-0.0032±~~0.0988 0.5~~0.0517	~~-0.0077~~-0.0025±~~0~~
$\tau_{plume} \sim 5.0$, ssa=0.8	-0.0035±0.0127	~~-0.0280~~0.0722±~~0.0907 0.0~~1.1557	~~-0.0072~~0.0023±~~0.0669 0.0~~0.0602	~~-0.0073~~-0.0021±~~0~~
$\tau_{plume} \sim 5.0$, ssa=1.0	-0.0028±0.0088	~~-0.0345~~0.0177±~~0.0867 0.0~~0.0431	~~-0.0106~~-0.0055±~~0.0822 0.0~~0.0468	~~-0.0097~~-0.0059±~~0~~
A(0.0)-A(0.1)	-0.0013±0.0045	~~-0.0015~~0.0007±~~0.0195 0.0~~0.0097	~~-0.0110~~-0.0038±~~0.0195 0.0~~0.0299	~~-0.0132~~-0.0048±~~0~~
A(1.0)-A(0.1)	0.0060±0.0172	~~-0.0047~~0.0029±~~0.0334 0.0~~0.0170	~~0.0596~~0.0294±~~0.0516 0.0~~0.0359	~~0.0791~~0.0392±~~0.~~
		Not including off-band correction, Eq.1.		
$\theta_0 = 60°$	-0.0098±0.0129	~~0.0158~~-0.0074±~~0.1463 0.3~~0.0718	~~0.0531~~0.0196±~~0.1932 1.3~~0.0787	~~0.0584~~0.0242±~~0.~~
$\phi_0 = 0 - 270°$	~~-0.0001~~-0.0011±~~0.0027~~0.0028	~~-0.0096~~0.0053±~~0.0752 0.0~~0.0495	~~-0.0109~~-0.0094±~~0.08180.0~~0.1743	~~-0.0067~~-0.0113±~~0~~
BG aerosol	-0.0045±0.0089	~~-0.0109~~0.0057±~~0.1016 0.0~~0.0503	~~-0.0114~~-0.0011±~~0.0804 0.0~~0.0391	~~-0.0053~~-0.0045±~~0~~
$\tau_{plume} \sim 0.5$, ssa=0.8	0.0021±0.0033	~~-0.0038~~-0.0559±~~0.0361 0.0~~1.1549	~~-0.0088~~-0.0061±~~0.0499 0.0~~0.0334	~~-0.0107~~-0.0053±~~0~~
$\tau_{plume} \sim 0.5$, ssa=1.0	0.0012±0.0024	~~-0.0072~~-0.0516±~~0.0706 0.0~~1.1553	~~-0.0072~~-0.0080±~~0.0706 0.0~~0.0645	~~-0.0119~~-0.0084±~~0~~
$\tau_{plume} \sim 5.0$, ssa=0.8	0.0199±0.0263	~~-0.0533~~-0.0317±~~0.1480 0.3~~1.1579	~~-0.0696~~-0.0461±~~0.1604 0.03~~0.1675	~~-0.0928~~-0.0569±~~0~~
$\tau_{plume} \sim 5.0$, ssa=1.0	~~0.00109~~0.0109±0.0139	~~-0.0629~~-0.0261±~~0.1343 0.5~~1.1577	~~-0.0479~~-0.0253±~~0.1140 0.3~~0.0709	~~-0.0595~~-0.0322±~~0~~
A(0.0)-A(0.1)	-0.0013±0.0043	~~0.0003~~-0.0002±~~0.0158 0.0~~0.0079	~~-0.0103~~-0.0039±~~0.0181 0.0~~0.0288	~~-0.0131~~-0.0051±~~0~~
A(1.0)-A(0.1)	0.0057±0.0171	~~-0.0033~~0.0022±~~0.0330 0.0~~0.0168	~~0.0626~~0.0301±~~0.0521 0.0~~0.0445	~~0.0822~~0.0419±~~0.~~

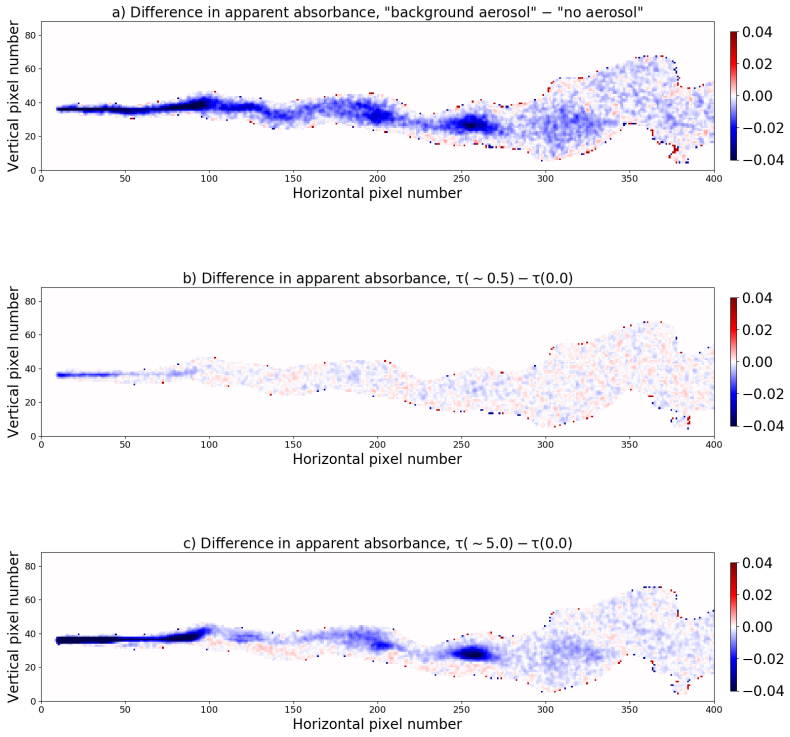

Figure 10. The difference in apparent absorbance from images recorded (a) with and without background aerosols in the atmosphere; (b-c) with and without aerosol in the plume (b): $\tau_{plume} \sim 0.5$; (c): $\tau_{plume} \sim 5.0$.

For the more realistic value, $\tau_{plume} \sim 0.5$, Fig. 10b, there is little impact on the apparent absorbance. For (non-)absorbing aerosol with ssa=0.8 (ssa=1.0) the decrease is less than 0.2% (0.16%) on average with off-band correction, and the increase is less than 1.1% (0.63%) on average without off-band correction. For (unrealistically) large amounts of (non-)absorbing aerosol in the plume, $\tau_{plume} \sim 5.0$, the apparent absorbance decreases by less than 2% (1.5%) on average if off-band correction is included, Eq. 2. Without off-band correction, Eq. 1, the apparent absorbance increases by 9.5% (5.43%) on average. For all cases, the off-band correction reduces the influence of aerosol, as intended. For both aerosol in plume cases and whether the off-band correction was included or not, the plume statistics were affected to a negligible extent, as reported in rows labeled "τ_{plume}" in Table 3. However, the standard deviation of the skewness increase largely when aerosol influence are not corrected for, or if the plume is thick and absorbing.

The sensitivity of the solar azimuth angle when including aerosols was investigated by performing additional simulations for $\phi_0 = 45$ and 180° for the aerosol in the plume and background aerosol cases with $\tau_{plume} \sim 0.5$. The solar azimuth angle sensitivity for these cases were of the same magnitude as for the aerosol free simulations and thus of negligible impact.

3.4 Surface albedo

All simulations above were made with a surface albedo $A = 0.0$ to avoid coupling between the various processes that affect the camera images. For the wavelengths considered here the albedo for snow-free surfaces is generally small ($A < 0.1$, see for example Wendisch et al., 2004). To test the sensitivity to snow free surface albedo, simulations were made for surface albedos of $A = 0.05$ and $A = 0.1$. In addition a simulation was made with $A = 1.0$ to estimate the effect of fresh snow which has a an albedo close to one at UV wavelengths (Wiscombe and Warren, 1980). The background images were calculated for each individual case. The apparent absorbance difference for the A(0.0)-A(0.1) and A(1.0)-A(0.1) cases are shown in Fig. 11. The

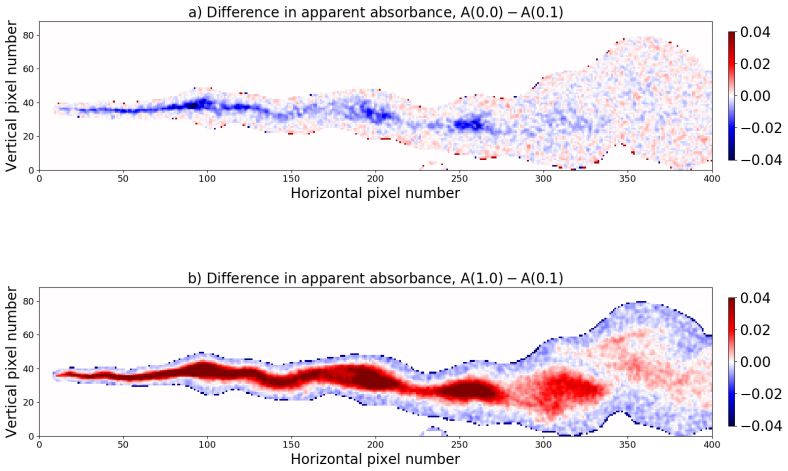

Figure 11. The difference in apparent absorbance from images recorded with surface albedo of (a) A(0.0) and A(0.1) and (b) A(1.0) and A(0.1).

overall results are summarized in Table 3. Decreasing the albedo from 0.1 to 0.0 gives an overall reduction in the apparent absorbance (mostly blue colors in Fig. 11a). Compared to the $A = 0.1$ case , the $A = 0.05$ case, not shown, is about a factor of 2 smaller in magnitude for the mean apparent absorbance. Increasing the albedo from 0.1 to 1.0 gives an increase in the apparent absorbance (mostly red colors in Fig. 11b). As mentioned above, section 3.2, the apparent absorbance is due to photons travelling along straight lines passing through the plume and into the camera. However, photons scattered between the plume and the camera, and multiple scattered photons within the plume, termed the light dilution and multiple scattering effect, respectively, may distort the apparent absorbance (Kern et al.). An additional distortion, not discussed by Kern et al., is due to the surface albedo which gives additional photon paths that may contribute to the camera signal. Some photons may scatter off the surface into the plume and in the direction of the camera. This will give increased (decreased) apparent absorbance with increasing (decreasing) albedo for relatively large SO_2 concentration, see red (blue) signal in Fig. 11b (a). For small SO_2 concentrations, the light dilution effect prevails, giving a reduction (increase) in the apparent absorbance for

increasing (decreasing) albedo, see blue (red) signal in Fig. 11b (a). While albedo changes may both increase and decrease the apparent absorbance, the impact on plume statistics is minor. Thus, overall, the surface albedo has negligible effect on the plume statistics (Table 3).

3.5 ~~Fractal dimension~~

~~The mass box-counting method, see section ??, was applied to seven random time frames (see Table 2) of LES-densities as exemplified in Fig. 1b and corresponding apparent absorbances from the radiative transfer simulation images for the reference situation (Fig. 3c). The mean D_{box} values for all LES-densities and radiative transfer simulation images were 1.170 and 1.156, respectively. In general there is no simple relationship between trace gas concentrations and the camera radiances as these are connected via the radiative transfer equation. Hence, the fractal dimensions of concentration fields and images may differ. The slightly lower dimension of the images may indicate that some radiative smoothing effect implies a loss of heterogeneity.~~

~~We note that Sykes and Gabruk (1994) report fractal dimension between 1.3 and 1.35 from area-perimeter and box-counting analysis for LES calculations representing neutral and convective conditions. Their results are for a different cross-section of the plume than the results presented here, namely the y-z plane in our coordinate system, Fig. 2. Furthermore, we analyse integrated line paths while they studied concentration. Thus, in their case a more heterogeneous surface may be expected.~~

4 Conclusions

~~Turbulence is one of the unsolved problems of physics.~~ One novel method to measure atmospheric turbulent tracer dispersion is to use UV cameras sensitive to absorption of sun-light by SO_2. In this paper we have presented a method to simulate such UV camera measurement with a 3D Monte Carlo radiative transfer model. Input to the radiative transfer simulations are large eddy simulations (LES) of a SO_2 plume. From the simulated images various plume density statistics (centerline position, meandering, absolute and relative dispersions, skewness~~, fractal dimension~~) were calculated and compared with similar quantities directly from the LES. Mean differences between the simulated images and the LES were generally found to be smaller ~~than a quarter of a pixel, with standard deviations between 1/2 and 3/2 pixel~~or about the size of the voxel resolution of the LES for the centerline. For the higher order statistics the differences increase as the SO_2 absorption gets weaker for a more and more dispersed plume.

Furthermore sensitivity studies were made to quantify how changes in solar azimuth and zenith angles, aerosol (background and in plume), and surface albedo, impact the UV camera image plume statistics. It was found that changing the parameters describing these effects within realistic limits, had negligible effect on the centerline position, meandering, absolute and relative dispersions, and skewness of the SO_2 plume.

~~Thus, based~~ Based on the simulated UV camera images and the comparison with the LES, it can be concluded that UV camera images of SO_2 plumes may be used to derive plume statistics of relevance for the study of atmospheric turbulence.

Code availability. The libRadtran software used for the radiative transfer simulations is available from www.libradtran.org. The PALM model system was used for the LES and it is available from palm.muk.uni-hannover.de/trac.

Author contributions. AK performed the radiative transfer simulations. HA, MC and SYP were responsible for the LES. AK prepared the manuscript with contributions from all co-authors.

Competing interests. The authors declare that no competing interests are present.

Acknowledgements. The Comtessa project has received funding from the European Research Council (ERC) under the European Union's Horizon 2020 research and innovation programme under grant agreement no. 670462. The resources for the numerical simulations and data storage were provided by UNINETT Sigma2 - the National Infrastructure for High Performance Computing and Data Storage in Norway under projects NN9419K and NS9419K.

References

Anderson, G., Clough, S., Kneizys, F., Chetwynd, J., and Shettle, E.: AFGL atmospheric constituent profiles (0-120 km), *Tech. Rep. AFGL-TR-86-0110*, Air Force Geophys. Lab., Hanscom Air Force Base, Bedford, Mass., 1986.

Ardeshiri, H., Cassiani, M., Park, S., Stohl, A., I.Pisso, and Dinger, A.: On the convergence and capability of large eddy simulation for passive plumes concentration fluctuations in an infinite-Re neutral boundary layer, Boundary-Layer Meteorol., xx, xx–xx, 2020.

Brown, R. J. and Bilger, R. W.: An experimental study of a reactive plume in grid turbulence, Journal of Fluid Mechanics, 312, 373–407, https://doi.org/10.1017/S0022112096002054, 1996.

Buras, R. and Mayer, B.: Efficient unbiased variance reduction techniques for Monte Carlo simulations of radiative transfer in cloudy atmospheres: The solution, J. Quant. Spectrosc. Radiat. Transfer, 112, 434–447, doi:10.1016/j.jqsrt.2010.10.005, 2011.

Cassiani, M., Stohl, A., and Eckhardt, S.: The dispersion characteristics of air pollution from the world's megacities, Atmospheric Chemistry and Physics, 13, 9975–9996, https://doi.org/10.5194/acp-13-9975-2013, https://www.atmos-chem-phys.net/13/9975/2013/, 2013.

Celik, I., Klein, M., and Janicka, J.: Assessment measures for engineering les application, J. Fluid Eng, 131(3), 031 102, 2009.

Deardorff, J.: The use of subgrid transport equations in a three-dimensional model of atmospheric turbulence, J. Fluid Eng, 95, 429–438, 1973.

Dinger, A. S., Stebel, K., Cassiani, M., Ardeshiri, H., Bernardo, C., Kylling, A., Park, S.-Y., Pisso, I., Schmidbauer, N., Wasseng, J., and Stohl, A.: Observation of turbulent dispersion of artificially released SO_2 puffs with UV cameras, Atmospheric Measurement Techniques, 11, 6169–6188, https://doi.org/10.5194/amt-11-6169-2018, https://www.atmos-meas-tech.net/11/6169/2018/, 2018.

Dosio, A. and de Arellano, J. V.-G.: Statistics of Absolute and Relative Dispersion in the Atmospheric Convective Boundary Layer: A Large-Eddy Simulation Study, Journal of the Atmospheric Sciences, 63, 1253–1272, https://doi.org/10.1175/JAS3689.1, http://dx.doi.org/10.1175/JAS3689.1, 2006.

Emde, C., Buras, R., Mayer, B., and Blumthaler, M.: The impact of aerosols on polarized sky radiance: model development, validation, and applications, Atmos. Chem. Phys., 10, 383–396, http://www.atmos-chem-phys.net/10/383/2010/, 2010.

Emde, C., Buras-Schnell, R., Kylling, A., Mayer, B., Gasteiger, J., Hamann, U., Kylling, J., Richter, B., Pause, C., Dowling, T., and Bugliaro, L.: The libRadtran software package for radiative transfer calculations (version 2.0.1), Geoscientific Model Development, 9, 1647–1672, https://doi.org/10.5194/gmd-9-1647-2016, http://www.geosci-model-dev.net/9/1647/2016/, 2016.

Feder, J.: Fractals, Plenum Press, New York, iSBN 0-306-42851-2, 1988.

Fossum, H. E., Reif, B. A. P., Tutkun, M., and Gjesdal, T.: On the Use of Computational Fluid Dynamics to Investigate Aerosol Dispersion in an Industrial Environment: A Case Study, Boundary-Layer Meteorology, 144, 21–40, https://doi.org/10.1007/s10546-012-9711-z, https://doi.org/10.1007/s10546-012-9711-z, 2012.

Gant, S. and Kelsey, A.: Accounting for the effect of concentration fluctuations on toxic load for gaseous releases of carbon dioxide, Journal of Loss Prevention in the Process Industries, 25, 52 – 59, https://doi.org/https://doi.org/10.1016/j.jlp.2011.06.028, http://www.sciencedirect.com/science/article/pii/S0950423011001094, 2012.

Gliß, J., Stebel, K., Kylling, A., and Sudbø, A.: Improved optical flow velocity analysis in SO_2 camera images of volcanic plumes – implications for emission-rate retrievals investigated at Mt Etna, Italy and Guallatiri, Chile, Atmospheric Measurement Techniques, 11, 781–801, https://doi.org/10.5194/amt-11-781-2018, https://www.atmos-meas-tech.net/11/781/2018/, 2018.

Hermans, C., Vandaele, A., and Fally, S.: Fourier transform measurements of SO_2 absorption cross sections:: I. Temperature dependence in the 24 000-29 000 cm^{-1} (345-420 nm) region, Journal of Quantitative Spectroscopy and Radiative Transfer, 110, 756–765,

https://doi.org/http://dx.doi.org/10.1016/j.jqsrt.2009.01.031, http://www.sciencedirect.com/science/article/pii/S0022407309000375, {HITRAN}, 2009.

Hilderman, T., Hrudey, S., and Wilson, D.: A model for effective toxic load from fluctuating gas concentrations, Journal of Hazardous Materials, 64, 115 – 134, https://doi.org/https://doi.org/10.1016/S0304-3894(98)00247-7, http://www.sciencedirect.com/science/article/pii/S0304389498002477, 1999.

Karperien, A.: FracLac for ImageJ, Tech. rep., National Institutes of Health, USA, http://rsb.info.nih.gov/ij/plugins/fraclac/FLHelp/Introduction.htm, 1999-2013.

Kern, C., Deutschmann, T., Werner, C., Sutton, A. J., Elias, T., and Kelly, P. J.: Improving the accuracy of SO2 column densities and emission rates obtained from upward-looking UV-spectroscopic measurements of volcanic plumes by taking realistic radiative transfer into account, Journal of Geophysical Research: Atmospheres, 117, https://doi.org/10.1029/2012JD017936, http://dx.doi.org/10.1029/2012JD017936.

Kern, C., Deutschmann, T., Vogel, L., Wöhrbach, M., Wagner, T., and Platt, U.: Radiative transfer corrections for accurate spectroscopic measurements of volcanic gas emissions, Bull Volcanol, 72, 233–247, 2010a.

Kern, C., Kick, F., Lübcke, P., Vogel, L., Wöhrbach, M., and Platt, U.: Theoretical description of functionality, applications, and limitations of SO_2 cameras for the remote sensing of volcanic plumes, Atmospheric Measurement Techniques, 3, 733–749, https://doi.org/10.5194/amt-3-733-2010, http://www.atmos-meas-tech.net/3/733/2010/, 2010b.

Kern, C., Werner, C., Elias, T., Sutton, A. J., and Lübcke, P.: Applying UV cameras for SO2 detection to distant or optically thick volcanic plumes, Journal of Volcanology and Geothermal Research, 262, 80–89, https://doi.org/http://dx.doi.org/10.1016/j.jvolgeores.2013.06.009, http://www.sciencedirect.com/science/article/pii/S0377027313001832, 2013.

Kylling, A., Buras, R., Eckhardt, S., Emde, C., Mayer, B., and Stohl, A.: Simulation of SEVIRI infrared channels: a case study from the Eyjafjallajökull April/May 2010 eruption, Atmospheric Measurement Techniques, 6, 649–660, https://doi.org/10.5194/amt-6-649-2013, http://www.atmos-meas-tech.net/6/649/2013/, 2013.

Lateb, M., Meroney, R., Yataghene, M., Fellouah, H., Saleh, F., and Boufadel, M.: On the use of numerical modelling for near-field pollutant dispersion in urban environments - A review, Environmental Pollution, 208, 271–283, https://doi.org/https://doi.org/10.1016/j.envpol.2015.07.039, http://www.sciencedirect.com/science/article/pii/S0269749115003723, special Issue: Urban Health and Wellbeing, 2016.

Lübcke, P., Bobrowski, N., Illing, S., Kern, C., Alvarez Nieves, J. M., Vogel, L., Zielcke, J., Delgado Granados, H., and Platt, U.: On the absolute calibration of SO_2 cameras, Atmospheric Measurement Techniques, 6, 677–696, https://doi.org/10.5194/amt-6-677-2013, http://www.atmos-meas-tech.net/6/677/2013/, 2013.

Maronga, B., Gryschka, M., Heinze, R., Hoffmann, F., Kanani-Sühring, F., Keck, M., Ketelsen, K., Letzel, M. O., Sühring, M., and Raasch, S.: The Parallelized Large-Eddy Simulation Model (PALM) version 4.0 for atmospheric and oceanic flows: model formulation, recent developments, and future perspectives, Geoscientific Model Development, 8, 2515–2551, https://doi.org/10.5194/gmd-8-2515-2015, https://www.geosci-model-dev.net/8/2515/2015/, 2015.

Mayer, B. and Kylling, A.: Technical note: the libRadtran software package for radiative transfer calculations-description and examples of use, Atmos. Chem. Phys., 5, 1855–1877, 2005.

Mayer, B., Hoch, S. W., and Whiteman, C. D.: Validating the MYSTIC three-dimensional radiative transfer model with observations from the complex topography of Arizona's Meteor Crater, Atmos. Chem. Phys., 10, 8685–8696, 2010.

Moeng, C.: A large-eddy simulation model for the study of planetary boundary-layer turbulence, J. Atmos. Sci, 41, 2052–2062, 1984.

Mori, T. and Burton, M.: The SO2 camera: A simple, fast and cheap method for ground-based imaging of SO2 in volcanic plumes, Geophysical Research Letters, 33, https://doi.org/10.1029/2006GL027916, https://agupubs.onlinelibrary.wiley.com/doi/abs/10.1029/2006GL027916, 2006.

Pope, S. B.: Turbulent Flows, Cambridge University Press, 2000.

Raasch, S. and Schröter, M.: PALM A large-eddy simulation model performing on massively parallel computers, Meteorologische Zeitschrift, 10, 363–372, https://doi.org/doi:10.1127/0941-2948/2001/0010-0363, https://www.ingentaconnect.com/content/schweiz/mz/2001/00000010/00000005/art00001, 2001.

Rasband, W.: ImageJ, Tech. rep., U. S. National Institutes of Health, Bethesda, Maryland, USA, https://imagej.nih.gov/ij/, 1997-2018.

Schauberger, G., Piringer, M., Schmitzer, R., Kamp, M., Sowa, A., Koch, R., Eckhof, W., Grimm, E., Kypke, J., and Hartung, E.: Concept to assess the human perception of odour by estimating short-time peak concentrations from one-hour mean values. Reply to a comment by Janicke etÂ al., Atmospheric Environment, 54, 624 – 628, https://doi.org/https://doi.org/10.1016/j.atmosenv.2012.02.017, http://www.sciencedirect.com/science/article/pii/S135223101200132X, 2012.

Stull, R. B.: An Introduction to Boundary Layer Meteorology, Kluwer Academic Publishers, Boca Raton, 1988.

Sykes, R. I. and Gabruk, R. S.: Fractal Representation of Turbulent Dispersing Plumes, Journal of Applied Meteorology, 33, 721–732, https://doi.org/10.1175/1520-0450(1994)033<0721:FROTDP>2.0.CO;2, https://doi.org/10.1175/1520-0450(1994)033<0721:FROTDP>2.0.CO;2, 1994.

Vilà-Guerau de Arellano, J., Dosio, A., Vinuesa, J.-F., Holtslag, A. A. M., and Galmarini, S.: The dispersion of chemically reactive species in the atmospheric boundary layer, Meteorology and Atmospheric Physics, 87, 23–38, https://doi.org/10.1007/s00703-003-0059-2, https://doi.org/10.1007/s00703-003-0059-2, 2004.

Wendisch, M., Pilewskie, P., Jäkel, E., Schmidt, S., Pommier, J., Howard, S., Jonsson, H. H., Guan, H., Schröder, M., and Mayer, B.: Airborne measurements of areal spectral surface albedo over different sea and land surfaces, J. Geophys. Res., 109, D08 203, doi:10.1029/2003JD004 393, 2004.

Wiscombe, W. J. and Warren, S. G.: A model for the spectral albedo of snow, I, Pure snow, J. Atmos. Sci., 37, 2712–2733, 1980.